© 2020. Published by The Company of Biologists Ltd | Development (2020) 147, dev193649. doi:10.1242/dev.193649

HUMAN DEVELOPMENT

RESEARCH ARTICLE

A molecular and cellular analysis of human embryonic optic fissure closure related to the eye malformation coloboma

Aara Patel[1], Glenn Anderson[2], Gabriel L. Galea[1], Monika Balys[2] and Jane C. Sowden[1,*]

ABSTRACT

Ocular coloboma is a congenital eye malformation, resulting from a failure in optic fissure closure (OFC) and causing visual impairment. There has been little study of the epithelial fusion process underlying closure in the human embryo and coloboma aetiology remains poorly understood. We performed RNAseq of cell populations isolated using laser capture microdissection to identify novel human OFC signature genes and probe the expression profile of known coloboma genes, along with a comparative murine analysis. Gene set enrichment patterns showed conservation between species. Expression of genes involved in epithelial-to-mesenchymal transition was transiently enriched in the human fissure margins during OFC at days 41-44. Electron microscopy and histological analyses showed that cells transiently delaminate at the point of closure, and produce cytoplasmic protrusions, before rearranging to form two continuous epithelial layers. Apoptosis was not observed in the human fissure margins. These analyses support a model of human OFC in which epithelial cells at the fissure margins undergo a transient epithelial-to-mesenchymal-like transition, facilitating cell rearrangement to form a complete optic cup.

KEY WORDS: Coloboma, Embryonic eye development, Optic fissure

INTRODUCTION

Ocular coloboma is a congenital eye malformation consisting of a ventrally located notch or gap in the iris, retina, choroid or optic nerve. Coloboma is often associated with microphthalmia (small under-developed eyes) (Shah et al., 2011) and accounts for 3.2 to 11.3% of cases of blindness in children (Onwochei et al., 2000). These conditions are genetically heterogeneous (Williamson and FitzPatrick, 2014; Reis and Semina, 2015; Patel and Sowden, 2017). Mutations in at least 39 human genes are associated with coloboma, although for most the number of cases identified is small. We recently showed that the majority (97%) of coloboma cases in a paediatric cohort were not explained by mutations in known genes (Patel et al., 2019). Better understanding of the genetic regulation of human eye morphogenesis will help the interpretation of genome-wide analysis of individuals with coloboma.

Human eye morphogenesis begins with the bilateral evagination of two optic vesicles from the neuroepithelium of the developing diencephalon, which invaginate asymmetrically to form bi-layered optic cups during the 5th week of gestation (O'Rahilly, 1983). The inner and outer layers differentiate into the neural retina (NR) and the retinal pigmented epithelium (RPE), respectively (Zagozewski et al., 2014). Initially the bi-layered optic cup has a fissure along its ventral aspect, known as the optic fissure, that eventually closes to create the complete eye globe. Coloboma occurs due to a failure in the process of optic fissure closure (OFC). Studies in vertebrate animal models, which have a similar but not identical eye morphogenesis to humans, have provided insights into underlying cellular and molecular processes. These studies have demonstrated that shaping of the optic cup and bringing the fissure margins into physical contact involves changing cell shape from apical to basal constriction (Nicolás-Pérez et al., 2016; Bogdanović et al., 2012), migration of cells from the outer to the inner layer (Heermann et al., 2015; Sidhaye and Norden, 2017), and different rates of cell proliferation in the two layers of the optic cup and along the dorso-ventral axis (Behesti et al., 2009; Kim et al., 2007). Invagination is preceded by patterning of the optic vesicle, based on the regional expression of transcription factors and gradients of signalling molecules (Patel and Sowden, 2017; Zagozewski et al., 2014; Fuhrmann, 2010). There is accumulating evidence of the way in which this patterning drives physical invagination (Behesti et al., 2006; Gago-Rodrigues et al., 2015).

Once the optic fissure margins (OFMs) are in contact, the neuroepithelium forming them fuses to form a continuous NR and RPE. This is one of many essential embryonic epithelial fusion processes, ranging from neural tube closure, palatogenesis and fusion of the semi-circular canal in vertebrates to dorsal closure in the *Drosophila* embryo, and involving the adhesion of two epithelial sheets and knitting together of their constituent cells. Epithelial remodelling typically involves cell neighbour exchange, apico-basal extension/contraction or junction matching. Cellular mechanisms directly associated with epithelial fusion include extension of actin-based filopodia and lamellipodia (Jacinto et al., 2000; Rolo et al., 2016), epithelial-to-mesenchymal transition (EMT), cell migration and apoptosis (Kim et al., 2015; Dudas et al., 2007; Fekete et al., 1997; Kobayashi et al., 2008). Yet the behaviour of the cells lining the OFMs is not well understood and has not been studied in human embryos. OFC may share cellular mechanisms with other epithelial fusion processes; however, there is one crucial difference: the cells approach each other from the basal aspect and therefore must first degrade, displace or break through the basement membrane to come in direct contact with each other. During neural tube closure, palatogenesis and semi-circular canal fusion, the epithelia approach each other from their apical aspects.

Several animal models of coloboma are characterised by a persistent basement membrane (Tsuji et al., 2012; Torres et al., 1996; See and Clagett-Dame, 2009) with the margins sometimes growing over each other (Tsuji et al., 2012; Barbieri et al., 2002). Other studies in mouse and zebrafish have suggested that cells originating from the periocular mesenchyme (POM) may play a role in basement membrane remodelling by releasing extracellular enzymes or phagocytosis (Hero, 1990; Hero et al., 1991; James et al., 2016). Electron microscopy in the mouse showed that cells

[1]UCL Great Ormond Street Institute of Child Health, and NIHR Great Ormond Street Hospital Biomedical Research Centre, University College London, London WC1N 1EH, UK. [2]Department of Histopathology, Great Ormond Street Hospital for Children NHS Foundation Trust, London WC1N 3JH, UK.

*Author for correspondence (j.sowden@ucl.ac.uk)

J.C.S., 0000-0003-0937-2479

Handling Editor: James Briscoe
Received 3 August 2020; Accepted 30 October 2020

Development (2020) 147, dev193649. doi:10.1242/dev.193649

lining the OFMs appear to extend cytoplasmic processes (Hero, 1990). Recent live imaging in the zebrafish reported that cells at the closure point transiently adopted protrusive morphologies (Gestri et al., 2018). Increased apoptosis has been observed in association with several closure processes. However, evidence for its role in optic fissure closure is contradictory and inconclusive (Van Nostrand et al., 2014; Lee et al., 2013; Noh et al., 2016; Gestri et al., 2018).

In summary, there are many open questions regarding cell behaviour at the OFMs. Whether and which animal model systems best represent cell behaviour in human embryos is unknown. Here, we present a new study of OFC in human embryos and examine patterns of gene expression at the OFMs using RNAseq to help resolve some of these questions and identify new disease candidate coloboma genes. We present evidence that cells lining the human optic fissure margins undergo EMT-like morphological changes at the time of fissure closure.

RESULTS

Optic fissure closure takes place bi-directionally during embryonic development

OFC in the human eye has previously been described to occur broadly between Carnegie stages (CS) 14 and 17 (O'Rahilly, 1983), which corresponds to 32 to 41 days post-ovulation (O'Rahilly and Muller, 1987). However, histology capturing the process of the human fissure closing to complete the eye globe is not available. Here, we performed a new histological analysis. Samples were obtained from the Human Developmental Biology Resource tissue bank (hdbr.org). Developmental ages of human embryos were approximated using morphological landmarks according to the Carnegie staging system (O'Rahilly and Muller, 1987) as more exact ages from conception cannot be determined for tissue donated from terminated pregnancies.

At CS15 (day 33), OFC had not started and POM cells were visible between the margins of the optic fissure (Fig. 1A-C; n=2 eyes from one embryo). The margins were aligned with each other but with a physical gap between them along their entire length. By CS16 (day 37) (n=3 eyes, from two embryos), the margins were in contact at a single point immediately posterior to the developing lens and closure had been initiated (Fig. 1D-F; Fig. S1A-F; see plate D). Closure at this stage only involved a few cells and had not extended across the thickness of the margins or progressed far anteriorly or posteriorly (Fig. 1G-I). Cells from the POM had been displaced from the fissure at the point of closure, but were still present between the margins anterior and posterior to this point. At CS17 (day 41), staining with an antibody against laminin (a marker of basement membrane; Byström et al., 2006; Chen et al., 2012) on serial sections (n=2 eyes from two embryos) showed the progression of fissure closure from the point of initiation. Discontinuous laminin staining was observed at the basal opposing surfaces where closure was in progress (Fig. 1K). Anterior and posterior to this, the fissure was still open with two intact basement membranes lining the margins (Fig. 1G,L, double arrows). At the extreme anterior of the optic cup, some POM cells were still present between the two margins (Fig. 1J). These analyses indicate that at CS17 fusion progresses bi-directionally toward the anterior and posterior poles from a midpoint of closure initiation. At CS18 (day 44), the fissure was open at the anterior of the cup (Fig. 1M) with an active point of closure immediately behind it, while OFC was complete closer to the point of initiation (Fig. 1N). The location of the point of initiation and directions of human OFC are shown in relation to the optic cup and anatomical planes in Fig. 1O,P.

The time scales of development in human and mouse embryos are very different. To compare gene expression in the two species, we identified time points equivalent in terms of the extent of OFC. Comparative analysis of mouse embryonic eyes based on series of histological sections of E11.5 (n=4) and E12.5 (n=3) eyes showed that at E11.5 closure had been initiated, as in human embryos, at a single point immediately posterior to the developing lens (Fig. S1G-L; see plate I). Anterior and posterior to this point, the fissure remained open (see high magnification view in Fig. S2A-C). Immunostaining for laminin showed that by E11.5 the basement membrane had begun to fragment at the point of closure (Fig. S2D-G), and by E12.5, fissure closure was nearly complete in all eyes (Fig. S2H-J). At the extreme posterior of the eyes there was a ventral indentation in the neural retina indicating where the fissure had just closed (Fig. S2J, arrow). Some marked morphological differences between species were also apparent at equivalent stages of OFC. In the mouse eye at E11.5, RPE maturation was more advanced than that in the human CS17 eye. It was already a thin mono-layer containing more pigment granules, whereas in the human it was thicker and closer in appearance to the pseudo-stratified inner neural layer of the optic cup (Fig. S2B, asterisk). In addition, in the mouse eye, the OFMs invert considerably into the fissure (Fig. S2A-C) more than in the human eye (Fig. 1K,L). These data showed that OFC occurred during day 41-44 of human embryonic development (CS17-CS18; weeks 6-7) and E11.5-12.5 in the mouse.

Laser capture microdissection and RNA-sequencing identified novel genes enriched at the OFC margins

We sought to identify gene expression signatures confined to the small group of cells at the fissure margins that are involved in OFC. The OFMs and a corresponding control region of dorsal optic cup were isolated using laser capture microdissection from human embryonic eyes and mouse embryos (Fig. S3A). This study design aimed to identify the signature of gene expression in the OFMs and to identify those genes that were more highly expressed along the ventral (inferior) fissure compared with the opposing dorsal (superior region). As day 41-44 embryos (CS17-18 stages) have active points of epithelial re-organisation and OFC they were considered suitable for transcriptomic analyses of the process of human fissure closure. Despite the scarcity of these OFC stage human samples, high-quality RNA was successfully isolated from microdissected regions for human (n=2 embryos at CS17, n=1 embryo at CS18) and mouse (n=3 embryos, six eyes, at E11.5 and E12.5) samples, and cDNA sequencing libraries prepared for RNAseq analysis.

Expression of 11 genes with previously known expression sites was interrogated to test the validity of data generated from the laser captured RNA samples. Six of these were known to be expressed strongly in the ventral optic cup (*SMOC1*/*Smoc1*, *PAX2*/*Pax2*, *ALDH1A3*/*Aldh1a3*, *VAX1*/*Vax1*, *VAX2*/*Vax2* and *BMP7*/*Bmp7*) (Okada et al., 2011; Torres et al., 1996; Dupe et al., 2003; Barbieri et al., 1999; Morcillo et al., 2006), and five in the dorsal optic cup (*TBX2*/*Tbx2*, *TBX3*/*Tbx3*, *TBX5*/*Tbx5*, *ALDH1A1*/*Aldh1a1* and *BMP4*/*Bmp4*) (Behesti et al., 2006; Matt et al., 2005). Three other genes (*VSX2*/*Vsx2*, *ATOH7*/*Atoh7* and *POU4F2*/*Pou4f2*) reported to be upregulated over time at the OFCs in mouse (Brown et al., 2009) were also included. Heatmaps for these genes showed the predicted differential expression pattern in the fissure margin and dorsal samples from both our human and mouse data (Fig. 2A,B), thereby validating the new datasets.

Expression patterns of previously reported human coloboma disease genes

We next evaluated the OFC expression patterns using our recently compiled set of 39 human coloboma disease genes and 23

Development (2020) 147, dev193649. doi:10.1242/dev.193649

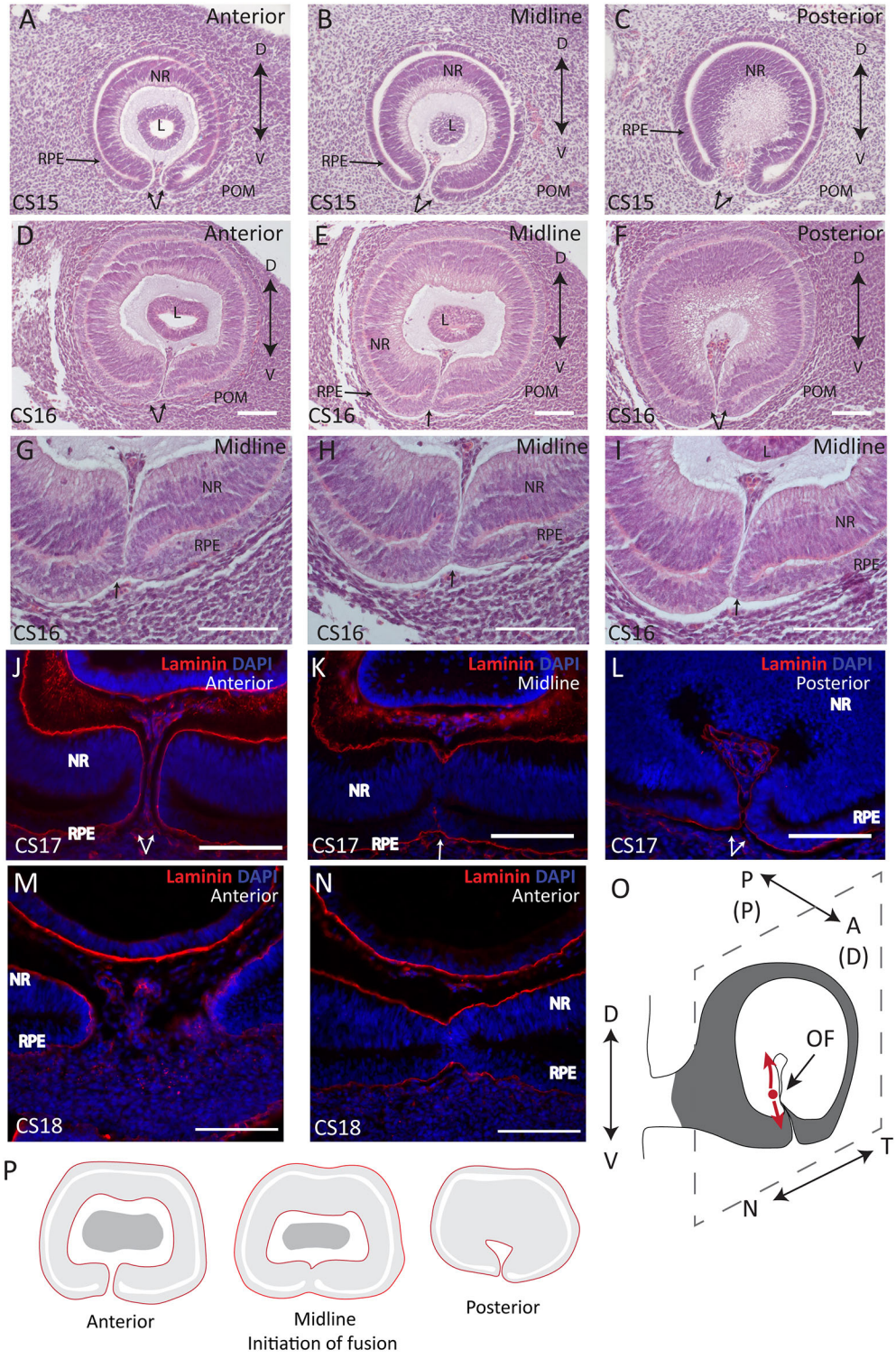

Fig. 1. Optic fissure closure is initiated at CS16 and progresses during CS17 and 18 in the developing human eye. (A-C) At Carnegie stage 15 (CS15) the OFMs approach each other but do not come in contact. POM cells are present between the margins along the length of the fissure (double arrows indicate the open fissure). (D-F) At CS16, the POM cells are displaced and closure is initiated at the mid-point of the fissure (E, arrow). Anterior and posterior to this point, POM cells are still present between the margins (D,F, double arrows indicate open fissure). (G-I) At the point of closure (arrow), fusion involves only a small number of cells at the folding point. (J-L) By CS17 (day 41) OFC has progressed at the mid-point and the basement membrane (stained for laminin) has dissolved (K, arrow). Anterior and posterior to this point it remains intact (J,L). (M,N) At CS18 (day 44), fissure closure is in progress at the anterior region of the developing eye (stained for laminin, red). (O,P) Schematics showing the initiation of OFC its bi-directional progress. Basement membrane, red; NR, neural retina (inner layer of optic cup); RPE, retinal pigmented epithelium (outer layer of optic cup); L, lens vesicle; POM, periocular mesenchyme. Scale bars: 100 µm.

additional candidate disease genes identified from animal models of coloboma (Patel and Sowden, 2017). Expression analysis during OFC has not previously been performed for most of these genes. Sixty were detected in our RNAseq analysis. Notably, this excluded coloboma genes *RBP4* and *SHH*, which are known to be expressed outside of the optic cup in early development (Chou et al., 2015; Echelard et al., 1993). Expression of the 60 detected genes was plotted as a heat map with the human coloboma disease genes highlighted in red in Fig. 2C. Similar heatmaps were also generated using their orthologous genes in the mouse expression datasets at E11.5 and E12.5 (Fig. S4A,B). As expected (Patel and Sowden, 2017), a group of the coloboma disease genes showed differential expression across the dorsal-ventral axis of the optic cup, with enriched expression in the fissure region indicating that they may be important for OFC. A second group of coloboma genes do not show ventral enrichment and are instead expressed at higher levels in the dorsal region. They include human coloboma-associated genes such as *PAX6*, *VSX2*, *GDF6* and *RAX*, which have wider roles affecting

Development (2020) 147, dev193649. doi:10.1242/dev.193649

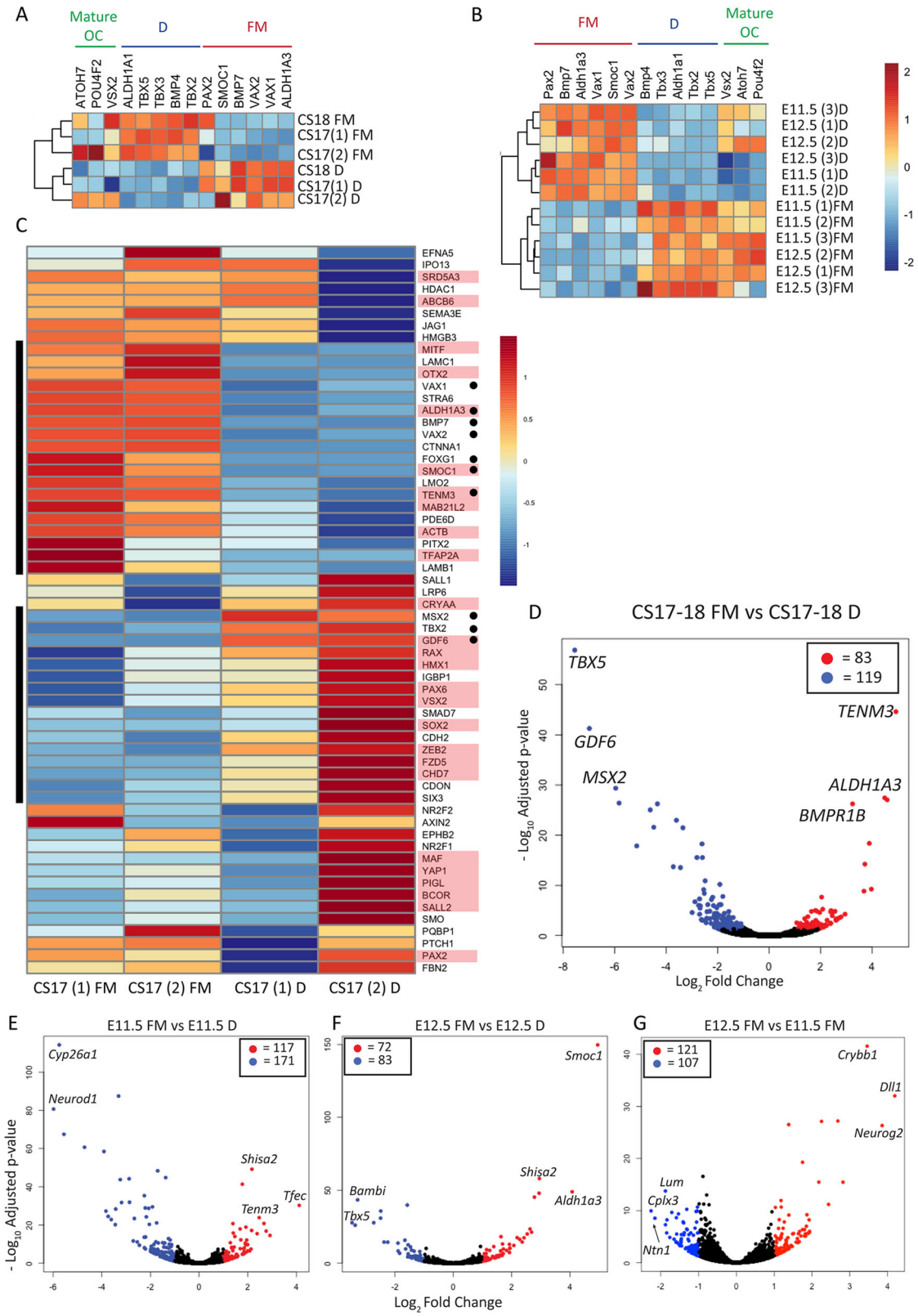

Fig. 2. Transcriptomic analysis of the closing optic fissure in human and mouse eyes. (A,B) Heatmaps showing expression of dorsal and ventral optic cup markers in the human and mouse micro-dissected RNA samples. Similar patterns of differential expression indicate conservation. (C) Heatmap showing expression of all coloboma-associated genes in the OFMs and dorsal regions from human CS17 eyes. Human coloboma disease genes are highlighted in red. Two groups of genes with either OFM- or dorsal-enriched expression are highlighted with a black bar, with those passing significance in subsequent differential expression analysis marked with a dot. (D-G) Volcano plots depicting all differential gene expression in the OFMs relative to the dorsal region in human embryonic eyes (n=3 embryos) and in E11.5 (C) and E12.5 (D) mouse eyes (n=3 embryos at each timepoint) and in the fissure margin region between E11.5 and E12.5 over the period of closure. Red, OFM-enriched genes; blue, OFM-downregulated genes/dorsal optic cup enriched (adjusted P<0.05, $\log_2$ FC≤−1). Table S6 shows the full list of differentially expressed genes.

Development (2020) 147, dev193649. doi:10.1242/dev.193649

the growth of the embryonic eye. The comparative analyses showed that more than half of the genes linked with coloboma fall into two distinct expression profile groups in both human and mouse, showing either fissure-enriched (FM) or dorsal-enriched (D, fissure-depleted) expression (CS17: FM=31.7%, D=26.7%, of 60 genes; E11.5: FM=27%, D=23.8%). These groups were smaller in the mouse at E12.5 (E12.5: FM=19%, D=9.5%). Other genes showed variable expression between samples, which may indicate a rapid temporal change in expression during fissure closure.

Differential gene expression analysis identified novel optic fissure margin- and dorsal-enriched genes sets in human and mouse

To identify additional genes that exhibit dorsal/fissure margin-enriched patterns of expression and therefore represent new candidate coloboma genes, a differential expression analysis was carried out (using adjusted $P<0.05$, Log2 FC≥1 as a cut off for significance, $n=3$ samples for each group). A comparison was also made between the mouse fissure margins at the two time points, as genes involved in the process of closure are likely to be dynamically regulated over this period.

In the human analysis at day 41-44 (CS17-18), 83 genes were significantly enriched at the fissure margins and 119 were significantly enriched in the dorsal optic cup (Fig. 2D). Table 1 shows the top 30 fissure- and dorsal-enriched genes in the human embryonic eyes (Fig. S5 shows a heatmap of the top 50 fissure- and dorsal-enriched genes). Table S6 shows all significantly differentially expressed genes with fold changes and *P*-values in all datasets analysed.

At E11.5 in the mouse, 117 genes were significantly enriched in the optic fissure margins and 171 were significantly enriched in the dorsal optic cup (Fig. 2E). At E12.5 the overall number of differentially expressed genes was smaller; 72 genes were significantly enriched at the fissure margins and 82 were significantly enriched in the dorsal optic cup (Fig. 2F). There was a partial overlap between these groups of genes: 23.9% of fissure-enriched genes at E11.5 remained fissure-enriched at E12.5; 17.5% of dorsal-enriched genes at E11.5 remained dorsal enriched at E12.5.

Tables S1 and S2 show the top 30 fissure- and dorsal-enriched genes in the mouse at the two time points along with a summary of the known functions of these genes based on gene ontology (GO) annotations. When the fissure margins at the two time points were compared, 121 genes were significantly upregulated over time and 107 were significantly downregulated (Fig. 2E). The genes showing the largest downregulation between E11.5 (beginning of OFC) and E12.5 (end of OFC) are *Cplx3*, *Ntn1*, *Lum*, *Tmem132c* and *Rgs13*. Those showing the largest upregulation are *Cryba4*, *Gadd45g*, *Cdh4*, *Stk33* and *Olfm1*.

To perform a comparative analysis between species, the mouse genes were converted to their human orthologues and compared with the list of significantly differentially expressed genes from the human fissure margins. Eleven genes (*TENM3*, *ALDH1A3*, *VAX1*, *BMP7*, *TFEC*, *VAX2*, *ZNF503*, *APOE*, *ABCA4*, *ATP1A2* and *SMOC1*) were significantly enriched in the fissure margins both in the human analysis and in the mouse analyses at either timepoint (Fig. 3A). Thirty-three genes showed significant dorsal enrichment in both species (*UNC5B*, *EFNB1*, *GDF6*, *CTNNA2*, *ID1*, *TBX2*, *EFNB2*, *ALDH1A1*, *BAMBI*, *FGF8*, *LPHN2*, *TBX3*, *EDIL3*, *NOL4*, *HES5*, *INSM1*, *NRCAM*, *DIAPH2*, *GADD45A*, *DKK3*, *SULF2*, *TOX*, *BMP4*, *SEMA3A*, *DCC*, *ASCL1*, *CAMK2N1*, *MAB21L1*, *MSX2*, *DTX4*, *ID4*, *TBX5* and *DCLK1*) (Fig. 3A). Of these 44 genes, mutations in five are known causes of human coloboma (*ALDH1A3*, *TENM3* and *SMOC1* – ventrally enriched; *GDF6* and *MSX2* – dorsally enriched) and four are homologues of genes that, when mutated, are known to cause coloboma in animal models (*BMP7*, *VAX2* and *VAX1* – ventrally enriched; *TBX2* – dorsally enriched) (Patel and Sowden, 2017; Williamson and FitzPatrick, 2014).

The identification of 44 genes showing conserved expression patterns between species was in line with the observation that the process of OFC appeared to be morphologically similar in mouse and human eyes. We used qRT-PCR to assess the expression of five of these genes (*ALDH1A3*, *SMOC1*, *ATP1A2*, *TENM3* and *TBX5*) and confirmed differential expression patterns of the human genes that was consistent with the RNAseq analysis (Fig. 3B). The qRT-PCR validation indicated that the RNAseq analysis was informative. The fact that the overlap between human and mouse genes was relatively low (22%; 44/202 differentially expressed human genes identified) may be explained by the dynamic gene expression observed during the OFC process, the variability in sample age and number available for RNAseq, and the significance thresholds selected. Owing to the limited availability of human samples it was not possible to analyse additional samples or validate multiple disease candidate genes in this study; however, these new data provide a resource for future studies.

Biological pathways represented by optic fissure-enriched genes were consistent between human and mouse

We found that the significantly enriched gene sets, in both species, were annotated with similar GO biological process terms. Fig. 3C shows Revigo semantic plots representing the most enriched GO terms; both species contained similar terms covering biological processes such as cell adhesion, axon guidance and Wnt signalling (also see Tables S3 and S4). Notably, the genes annotated in the two species were often different, which may be due to incomplete GO annotations, or because some differentially expressed genes did not pass the significance thresholds. For example, for the cadherin superfamily of cell-adhesion molecules (Paulson et al., 2014), in the mouse gene set cadherin 4 (*Cdh4*) and the protocadherin genes (*Pcdh17* and *Pcdh19*) were significantly downregulated at the fissure margins, while in the human gene set, *CDH6* was significantly downregulated. *Cdh4*, also known as r-cadherin (Babb et al., 2005, Liu et al., 2001), and *Pcdh17* have been implicated in retinal differentiation (Chen et al., 2013b), whereas a closely related cadherin, *Cdh2* (N-cad), has previously been implicated in coloboma, with disrupted retinal lamination, in zebrafish (Masai et al., 2003).

Gene set enrichment analysis showed conservation of pathways, including enrichment of gene expression involved in EMT in the fissure margins that coincides with closure

A complementary approach, gene set enrichment analysis (GSEA), was used to analyse signatures of biological processes in the entire transcriptomes of the fissure margins (Subramanian et al., 2005). GSEA showed conservation of pathways between the two species. The mouse early time point (E11.5) and human (CS17-18) shared the largest number of significantly positively (20) as well as negatively (4) correlated gene sets (Table S5). In addition, a number of gene sets were significantly positively correlated with the human CS17-18 fissure margins that did not show significant correlation in the mouse (Table S5).

Among the gene sets significantly correlated with OFC is the epithelial mesenchymal transition (EMT) gene set, which is of interest in relation to fissure closure because of the emerging evidence of transient changes in cell shape occurring at the fissure margins in the chick and zebrafish (Bernstein et al., 2018; Gestri et al., 2018) (Fig. 3D). The EMT gene set was positively correlated with the optic fissure region in the E11.5 mouse expression dataset (NES=1.47,

Development (2020) 147, dev193649. doi:10.1242/dev.193649

Table 1. Fissure- and dorsal-enriched genes in CS17-18 human eyes

Gene	Eye development	Regulation of transcription	Extracellular matrix related	Endocytosis/ phagocytosis	Regulation of apoptosis	Neuron projection related	Cell adhesion	Cytoskeleton related	EMT	Fold change	Adjusted *P*-value
*TENM3**,‡	Y					Y	Y			30.51	2.455E-45
*ALDH1A3**,‡	Y				Y					24.13	9.226E-28
MGC45800										22.57	3.717E-28
CD207				Y						15.76	5.662E-10
ATP6V1B1										14.90	4.375E-19
*VAX2**,‡	Y	Y				Y				13.24	5.930E-15
*VAX1**,‡	Y					Y				12.90	1.440E-09
BMPR1B	Y	Y	Y			Y				9.50	5.808E-27
CD93				Y			Y			7.75	5.667E-05
CLEC4F				Y						6.96	1.975E-04
*FOXG1**	Y					Y				6.63	2.977E-04
CDH5							Y			6.24	6.560E-04
NTN1					Y	Y	Y			6.07	9.073E-04
HCRT		Y								6.07	4.729E-04
THY1			Y			Y	Y	Y	Y	5.93	1.487E-05
SLIT3						Y				5.62	1.969E-05
PMEL										5.50	1.142E-04
SLC7A5						Y				5.32	1.061E-05
ATP1A2‡										5.27	1.969E-05
DDX60										5.27	3.567E-03
TM4SF18										5.25	3.783E-03
PAMR1			Y							5.24	3.653E-03
DCT										4.78	8.977E-04
CDC20B										4.71	1.017E-02
SCN3A										4.61	6.800E-03
FLT1										4.41	1.610E-02
ME3										4.41	1.379E-02
*SMOC1**,‡	Y									4.38	1.731E-02
F13A1										4.37	1.757E-02
ANKDD1B										4.37	1.938E-02
ZNF503‡		Y								3.91	2.62E-05
TFEC‡		Y								3.73	0.026593561
ABCA4‡										3.65	0.036523176
APOE‡			Y	Y		Y		Y		3.53	0.000950703
BMP7‡		Y	Y		Y	Y	Y		Y	3.49	1.01E-05
DKK3‡		Y								0.47	0.008349088
LPHN2‡										0.46	0.004809967
MAB21L1‡	Y									0.42	0.002884225
DIAPH2‡								Y		0.42	0.038423634
ID1‡		Y			Y					0.40	0.016708163
CAMK2N1‡										0.38	0.006938039
DTX4‡										0.36	0.002804427
SULF2‡										0.35	0.000477402
TOX‡										0.34	0.006994891
EFNB1‡							Y			0.30	0.037051527
SEMA3A‡						Y				0.29	0.002996199
GADD45A‡					Y					0.28	0.005550874
NOL4‡										0.26	0.021765781
HES5‡	Y	Y					Y			0.26	0.004129488
NRCAM‡						Y	Y			0.23	0.000234319
FGF8‡								Y	Y	0.23	0.019549469
BMP4‡		Y	Y		Y				Y	0.22	1.10E-06
DCLK1‡										0.21	6.80E-08
UNC5B‡										0.20	1.41E-05
KIAA1456										0.19	3.651E-04
CRYBA4	Y									0.18	2.777E-03
CNTN5							Y			0.18	1.257E-11
MIAT										0.18	3.887E-09
EDIL3‡			Y							0.17	7.267E-10
DCC‡					Y	Y				0.17	9.421E-04
CTNNA2‡						Y	Y	Y		0.17	2.926E-16
ID4‡		Y								0.16	5.593E-19
SLC16A6										0.16	8.977E-04
LGR6										0.16	6.776E-04
ASCL1‡		Y				Y				0.16	1.240E-06
GPR37										0.16	3.521E-06
PLP1						Y				0.15	5.911E-05

(Continued)

Development (2020) 147, dev193649. doi:10.1242/dev.193649

Table 1. (Continued)

Gene	Eye development	Regulation of transcription	Extracellular matrix related	Endocytosis/ phagocytosis	Regulation of apoptosis	Neuron projection related	Cell adhesion	Cytoskeleton related	EMT	Fold change	Adjusted *P*-value
HEY1		Y							Y	0.15	5.077E-08
COL23A1			Y							0.15	1.026E-06
IGFBPL1										0.14	2.895E-16
INSM1‡		Y								0.14	1.910E-07
SYT4										0.13	2.616E-05
EFNB2‡						Y	Y			0.10	3.354E-22
*TBX2**,‡		Y								0.09	2.886E-14
DKK1		Y			Y					0.08	1.092E-23
FIBCD1										0.08	1.953E-14
BAMBI‡									Y	0.05	5.808E-27
TF										0.04	2.653E-22
ALDH1A1‡										0.04	9.204E-26
TBX5-AS1										0.03	1.400E-18
*TBX3**,‡	Y	Y								0.02	4.074E-27
MSX2‡		Y			Y				Y	0.02	4.434E-30
*GDF6**,‡	Y				Y					0.01	5.406E-42
*TBX5**,‡	Y	Y							Y	0.01	1.356E-57

Fold changes >1 indicate fissure enrichment; <1 indicate enrichment in dorsal optic cup, for the top 30 genes, as well as additional genes that showed conserved patterns in mouse (between the single lines). Y indicates the presence of GO gene functions.

*Known coloboma genes (in humans or animal models). See also Fig. S5 showing a heatmap of the top 50 significantly enriched human genes.

‡Genes showing conserved human-mouse patterns.

P_{adj}=0.07) and in the CS17-18 human expression dataset (NES=1.54, P_{adj}=0.019) but was strongly negatively correlated in the mouse E12.5 dataset (NES=−1.78, P_{adj}=0.004). Enrichment plots for this gene set are shown in Fig. 3E. The E11.5 mouse and CS17-18 human datasets show an accumulation of EMT genes enriched in the fissure margins, while the E12.5 mouse dataset shows an accumulation of EMT genes enriched in the dorsal optic cup (and relatively depressed in the OFMs). In addition, three other gene sets showing a similar positive correlation with the fissure region at E11.5 in the mouse and CS17-18 in the human (mTORC1 signalling, PI3K-AKT-MTOR signalling and TNFA signalling via NFkB) represent signalling pathways known to regulate EMT in contexts other than the developing eye (Chua et al., 2007; Lamouille and Derynck, 2007; Medici and Nawshad, 2010) (Fig. 3C). Fig. 3F,G shows genes from the 'leading edge' of the EMT gene set in the human CS17-18 and mouse E11.5 datasets. These data suggest that a transient occurrence of an EMT-like process may facilitate OFC.

Notable examples include the following. *COL3A1/Col3a1*, a secreted component of the extracellular matrix (ECM) and a known marker of EMT (Zeisberg and Neilson, 2009) was enriched at the mouse and human (FC=2.4) OFMs. *Col3a1* is strongly expressed in mesenchymal tissue during mouse development (Niederreither et al., 1995) and enables the correct deposition of Type I collagen (Liu et al., 1997). Type I and Type III collagens were reported to be deposited during EMT (Gonzalez and Medici, 2014). In addition, *Col9a2* was dorsally enriched in the mouse and *COL11A1*, *COL22A1*, *COL9A3*, *COL13A1* and *COL25A1* were significantly dorsally enriched in the human. Expression of *LUM/Lum* (lumican), which encodes the leucine-rich proteoglycan ECM component lumican (Nikitovic et al., 2008) was enriched at the mouse optic fissure margins at E11.5 (FC=1.6) and strongly downregulated from E11.5 to E12.5 (FC=0.28, P_{adj}=1.73E^{-14}). Previous studies have implicated lumican in endothelial-mesenchymal transition, cell proliferation and cell adhesion and migration (Chakravarti et al., 2000). Expression of the cadherin gene *Cdh2/CDH2* was lower at the fissure margins than at the dorsal optic cup in both species. This is consistent with observations in the chick retina showing that Cdh2 expression is absent in a very distinct region around the fissure margins and in cells that delaminate from the fissure margins (Bernstein et al., 2018). However, it is contradictory to the generally accepted role of N-cadherin as a marker of the mesenchymal state (Gonzalez and Medici, 2014).

Immunostaining and electron microscopy show that cells at the point of OFC in the human eye display a marked change in morphology, consistent with transient EMT

Immunohistochemistry using antibodies against ZO-1, PAX6 and vimentin was used to investigate whether cells at the closing optic fissure transiently lose their epithelial characteristics during OFC: ZO-1 is a component of tight junctions (and helps form adherens junctions), which are lost in epithelia during EMT (Gonzalez and Medici, 2014); PAX6 is a transcription factor expressed in optic cup neuroepithelium; and vimentin is a cytoskeletal protein present in mesenchymal cells and considered to be one of the essential intermediate filaments for changes in cell shape (Franke et al., 1982; Wang et al., 2018). Prior to OFC, a line of ZO-1 staining was seen along the apical surface of the folding pseudostratified neuroepithelium at the OFM (Fig. 4A, arrowheads), and extended along the apical surface of both the presumptive NR and RPE; the ZO-1 staining appeared as a thick single line in regions where the apical surfaces were closely apposed (Fig. 4B). As OFC progressed, a disorganised group of cells, no longer stained apically by ZO-1, straddled the closing fissure region (Fig. 4C, dashed box region). Counterstaining for PAX6 suggested that this group of cells delaminated from the neuroepithelium of the optic cup, and not the POM (Fig. 4D). Once OFC was complete, neuroepithelial apical-basal polarity was re-established and two continuous lines of ZO-1 staining were seen across the remodelled NR and RPE (Fig. 4E).

Although punctate vimentin staining is characteristic of mesenchymal cells but not epithelia of the early mouse embryo and is often used as a marker of EMT (Franke et al., 1982), it has also been shown to label neural precursor cell processes. We observed intense spots of vimentin staining in the POM (Fig. 4A). Vimentin also labelled the basal aspect and processes of neuroepithelium cells beyond the fissure (Fig. 4B, asterisk). At the seam where the basal surfaces of the fissure margins approach each other, vimentin puncta were present (Fig. 4B,B′, arrowheads) and as cells at the OFC point round up and lose their neuroepithelial cell shape and

Development (2020) 147, dev193649. doi:10.1242/dev.193649

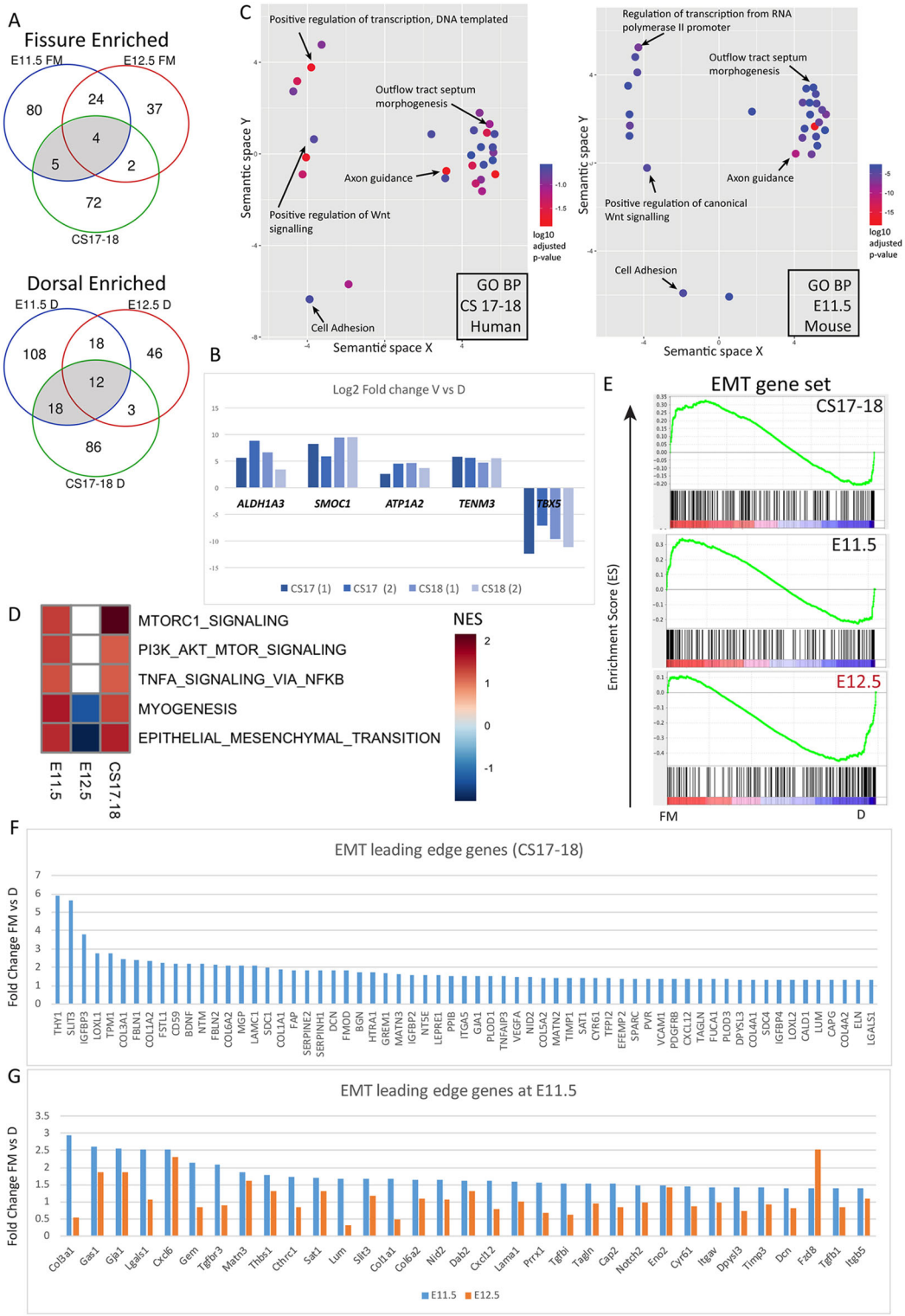

Fig. 3. Pathway analysis of differentially expressed genes. (A) Venn diagrams representing the genes significantly enriched in the fissure margin (FM) or dorsal (D) regions in mouse E11.5 and E12.5 eyes, and human CS17-18 eyes showing the overlaps between the two species. (B) qRT PCR validation of expression of selected genes in four samples [CS17 (1), CS17 (2), CS18 (1) and an additional sample CS18 (2)]. All samples showed fissure or dorsal enrichment of all selected genes, similar to the RNAseq analysis. (C) Semantic plots of biological process gene ontology terms in the differentially expressed genes (fissure and dorsal enriched) in the two species are similar. (D) A heat map showing the normalised enrichment score (NES) for hallmark gene sets related to epithelial-to-mesenchymal transition (EMT) across both species. Red, positively correlated; blue, negatively correlated; white, not passing significance. (E) Enrichment plots for the EMT gene set in relation to the fissure margin region. The enrichment score (ES), on the *y*-axis, is plotted against the list of the genes ranked by $\log_2$ fold change, on the *x*-axis, beginning with genes upregulated in the fissure margins and ending with genes downregulated in the margins. During fissure closure, there is a strong positive peak in the enrichment plot, with genes from the EMT gene set clustering towards the fissure margin end of the ranked gene list. The opposite is true for the later stage E12.5 mouse dataset. (F) Genes within the leading edge of the EMT gene set in human samples. (G) Genes within the leading edge of the EMT gene set at E11.5 and with their fold changes in the E12.5 mouse samples.

Development (2020) 147, dev193649. doi:10.1242/dev.193649

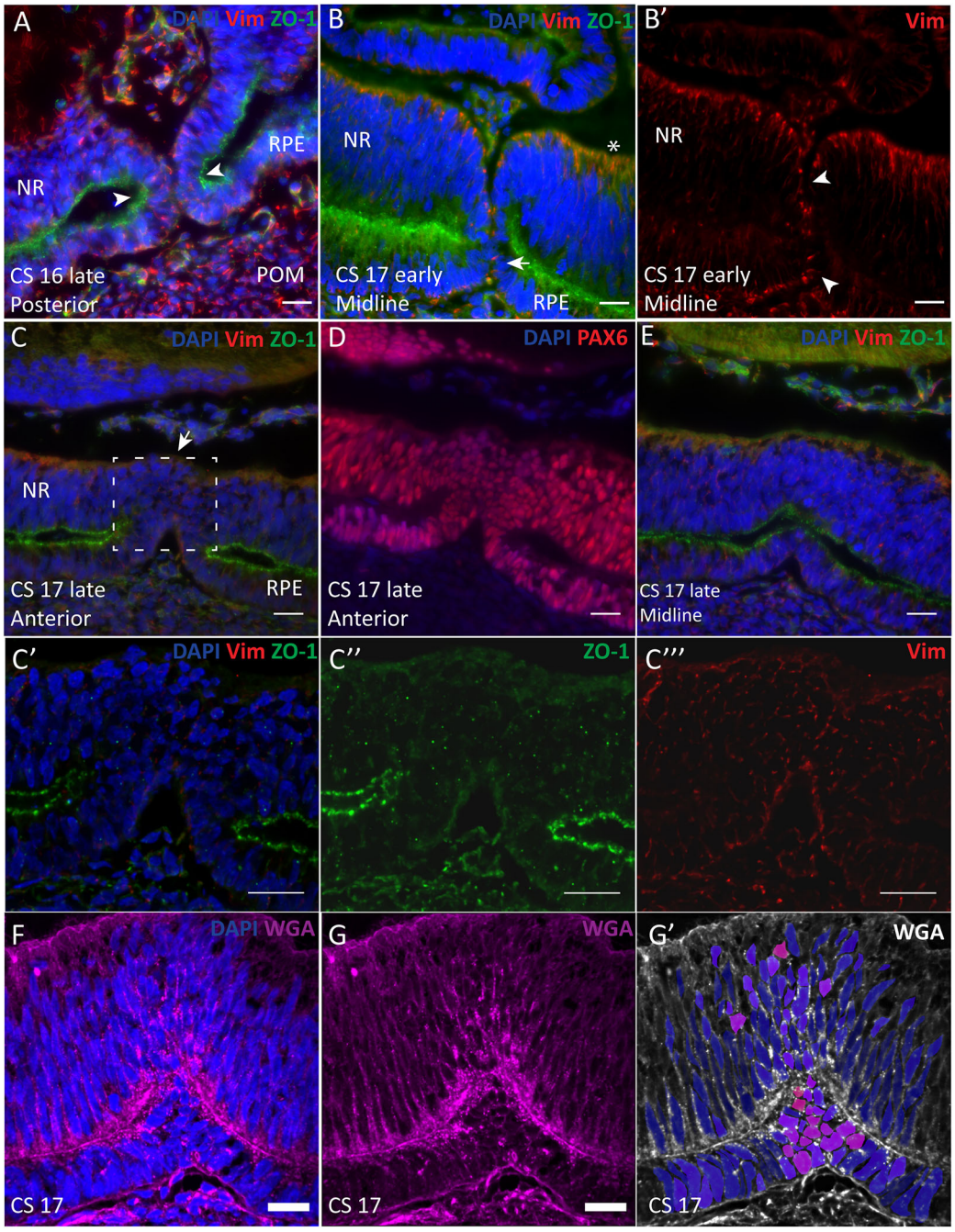

Fig. 4. Optic fissure margin cells express vimentin and de-laminate from the neuro-epithelium. (A-C) Expression of vimentin (a marker of mesenchymal cells) and ZO-1 (a marker of epithelial tight junctions) in the closing human optic fissure. In late CS16 and early CS17 eyes, fissure closure has initiated, but not completed; ZO-1 expression is interrupted across the fissure (A-B′). Arrowheads in A indicate Z0-1 staining at the apical surface of folding neuroepithelium; arrow in B indicates closure point. Vimentin expression is also seen in basal cells of the neural retina, facing the lens vesicle (asterisk). B′ shows a line of punctate vimentin expression in the cells at the point of closure, between white arrowheads. (C) A single line of ZO-1 staining along the apical surfaces of the neuroepithelium of the optic cup; before closure, this line folded over at each margin (arrow). (C′-C‴) High magnification single-channel views of the boxed region in C. The group of re-arranging cells at the point of closure display vimentin-positive puncta. (D) The rearranging cells (boxed in C) do not lose expression of PAX6, a marker of neuroepithelium of the optic cup. (E) Once closure is complete, ZO-1 staining becomes continuous across the fissure. (F,G) Labelling cell membranes with wheat germ agglutinin (WGA) shows that cells at the point of closure have a rounded morphology in contrast to elongated cells in the adjacent neuroepithelium. Cells are false coloured by roundness (G′). Red, round; blue, elongated. See also Fig. S6 showing the roundness heatmap in relation to adjacent sections and Movies 1–4 showing WGA with phalloidin immunohistochemistry as 3D projections. Scale bars: 100 µm in A-E; 20 µm in C′-C‴,F-G′.

polarity, punctate vimentin staining continues in reorganising cells (Fig. 4C, dashed box region, magnified view in Fig. 4C′-C‴). Fluorescently labelled wheat germ agglutinin (WGA) was used to label cell membranes (Fig. 4F,G) and then Fiji-based software was used to map the relative roundness of cells from deconvolved *z*-stacks. Roundness heatmaps were created (Fig. 4G′, pink indicates round cells, whereas blue indicates elongated cells; see also Fig. S6) confirming that cells at the point of closure adopted a rounded morphology, while those further away were elongated and typical of a pseudostratified epithelium. Fig. S6 shows heatmaps from different

Development (2020) 147, dev193649. doi:10.1242/dev.193649

regions during closure and Movies 1-4 show three-dimensional reconstructions of these cells.

Developing human eyes (n=2 individuals at CS17) were next studied in ultrastructural detail using Toluidine Blue-stained semi-thin sections and transmission electron microscopy (EM) to investigate if there was morphological evidence for an EMT-like change occurring during the process of OFC. Semi-thin sections near the point of closure showed that POM cells were displaced from in between the fissure margins (Fig. 5A). Prior to closure, the cells lining the OFMs had elongated nuclei similar to the remaining neural epithelium (Fig. S7A). However, cells at the point of closure differed in appearance from the rest of the cells in the NR or RPE. They were smaller with rounded nuclei and were not arranged in a layer, but formed a disorganised group (Fig. 5A, Fig. S7B). Where OFC had progressed further, a larger zone of cells with a rounded morphology spanning the thickness of the fissure was seen in between elongated epithelial cells at either side (Fig. 5B). EM at the point of closure showed rounded cells (yellow) alternating with elongated cells (blue) that possessed cell junctions, resembling immature tight junctions, at their apical ends (arrowhead). The rounded cells were located closer to the basal aspect of the epithelium (Fig. 5C,D, Fig. S7C). As the rounded cells alternate with elongated cells, it is unlikely that the former represent an epithelium in a different orientation (Fig. 5C).

In both eyes, some cytoplasmic material was extruded from the epithelial layer into the space between the fissure margins (Fig. 5C, arrow; Fig. S7D). The extruded material contained organelles that included mitochondria and was surrounded by a fragmented basement membrane, indicating that it originated from the neuroepithelium of the optic cup, rather than from trapped cells of the POM (Fig. S7D). It was not clear whether it included nuclei, i.e. whether whole cells or only parts of cells were being discarded. At higher magnification, cells could be seen extending cytoplasmic protrusions, which appeared to interact with cells from the opposite margin (Fig. 5E, arrowheads). These cells still maintained junctions at their apical ends (Fig. 5E, arrows). In addition, the basement membrane lining the margins appeared to break into fragments, which were seen among the rearranging cells at the point of closure. In regions where closure was complete, the cells had regained their elongated morphology and were arranged as a pseudo-stratified epithelium (Fig. 5F). Overall, the ultrastructural study suggested that the cells undergo a change in state from their original neuro-epithelial state once the POM cells are excluded and the margins come in contact with each other.

Immunostaining of the closing OFMs with phalloidin was used to determine whether the cell protrusions observed at the point of closure by EM analysis contained filamentous actin. Actin-rich foci have been recently described in the chick fissure margins (Bernstein et al., 2018). At the point of closure in an early CS17 human eye, a few cells showed strong puncta of actin staining (Fig. 6A,B, arrowheads). In the same eye in the open region of the fissure, cells in the OFMs approaching each other also showed strong puncta of actin staining (Fig. 6C,D arrowheads). At the points where the margins came in contact with each other, actin puncta were located at the basal aspects of the neuroepithelial closure points (Fig. 6E,F, arrowheads). Movie 4 shows phalloidin staining at the closing margin (green), counterstained with WGA (magenta). Cells of the neuroepithelium away from the fissure margins showed a more diffused pattern of actin staining. Antibody staining against PAX6 or PAX2 showed that the cells with punctate actin staining, displaying a mesenchymal morphology, originated from the neuroepithelium of the optic cup and not the POM (Fig. 6A,C). PAX6 was more prevalent in the anterior fissure and PAX2 more prevalent in the posterior fissure, consistent with data in the mouse (Chiang et al., 1996).

Taken together, these observations suggest that EMT-like changes in cell state occur at the human OFMs and that this is partial and transient. Eventually, as closure completes, the cells regain their epithelial organisation. There is increasing evidence in other systems for epithelial plasticity and that epithelial and mesenchymal states are not binary states (Nieto, 2013).

Apoptotic cell death is not associated with human OFC

Evidence regarding the involvement of apoptosis in OFC from studies in animal models is contradictory. Studies have described both too much and too little apoptosis resulting in coloboma in mouse and zebrafish models (Van Nostrand et al., 2014; Lee et al., 2013; Noh et al., 2016), or that apoptosis is dispensable for fissure closure in zebrafish (Gestri et al., 2018). Here, we did not find evidence associating apoptosis with human optic fissure closure from the RNAseq or histological analysis. Using an antibody specific for apoptotic marker cleaved caspase 3 (CC3) (Nicholson et al., 1995) apoptotic cells were observed in mouse eyes at E11.5 (n=2) and E12.5 (n=4) clustering around the optic fissure, which is consistent with reports in existing literature (Ozeki et al., 2000; Noh et al., 2016). However, no apoptotic cells were observed in human eyes (n=3 eyes) at CS17. A small number of apoptotic cells were identified in the developing lens. A possible explanation for this is that apoptosis is not essential for epithelial remodelling at the human fissure but occurs in some species because of cells transiently losing their epithelial arrangement (McLaughlin et al., 2007).

DISCUSSION

In this study, we investigated for the first time the cellular organisation and gene expression during human OFC alongside a comparative analysis of the mouse eye. The morphological analysis identified post-ovulation days 41-44 (CS17-18) as the stages during which fissure closure takes place, identifying the susceptibility period during which teratogenic or genetic insults may impair OFC and cause coloboma. Fig. 7 shows a schematic representation of cell behaviour at the human optic fissure margins based on our analysis.

Role of POM cells in basement membrane breakdown

POM cells were cleared from the fissure before basement membrane breakdown and the initiation of OFC in human embryos. These observations are consistent with the proposal that POM cells around the optic cup secrete factors that maintain the basement membrane (Hirai et al., 1992; Ekblom et al., 1994) and their absence at the fissure contributes to basement membrane breakdown. Conversely, it has been proposed in mouse and zebrafish that cells originating from the POM contribute to basement membrane breakdown by phagocytosis or secreting enzymes (Hero, 1990; Hero et al., 1991; James et al., 2016).

Genes enriched at the fissure margins support a change in cell state as a mechanism of closure

Novel genes identified at the fissure margins include potential regulators of cell morphology and the actin cytoskeleton. *NTN1* was one of these. In a separate study, we showed that *NTN1* expression in the fusing fissure margins is conserved across multiple species and is required for successful fissure closure (Hardy et al., 2019). NTN1 is a diffusible cell signalling molecule that can induce the extension of filopodia and lamellipodia in target cells (Deiner et al., 1997). It has been shown to induce EMT along with activation of NF-κB

Development (2020) 147, dev193649. doi:10.1242/dev.193649

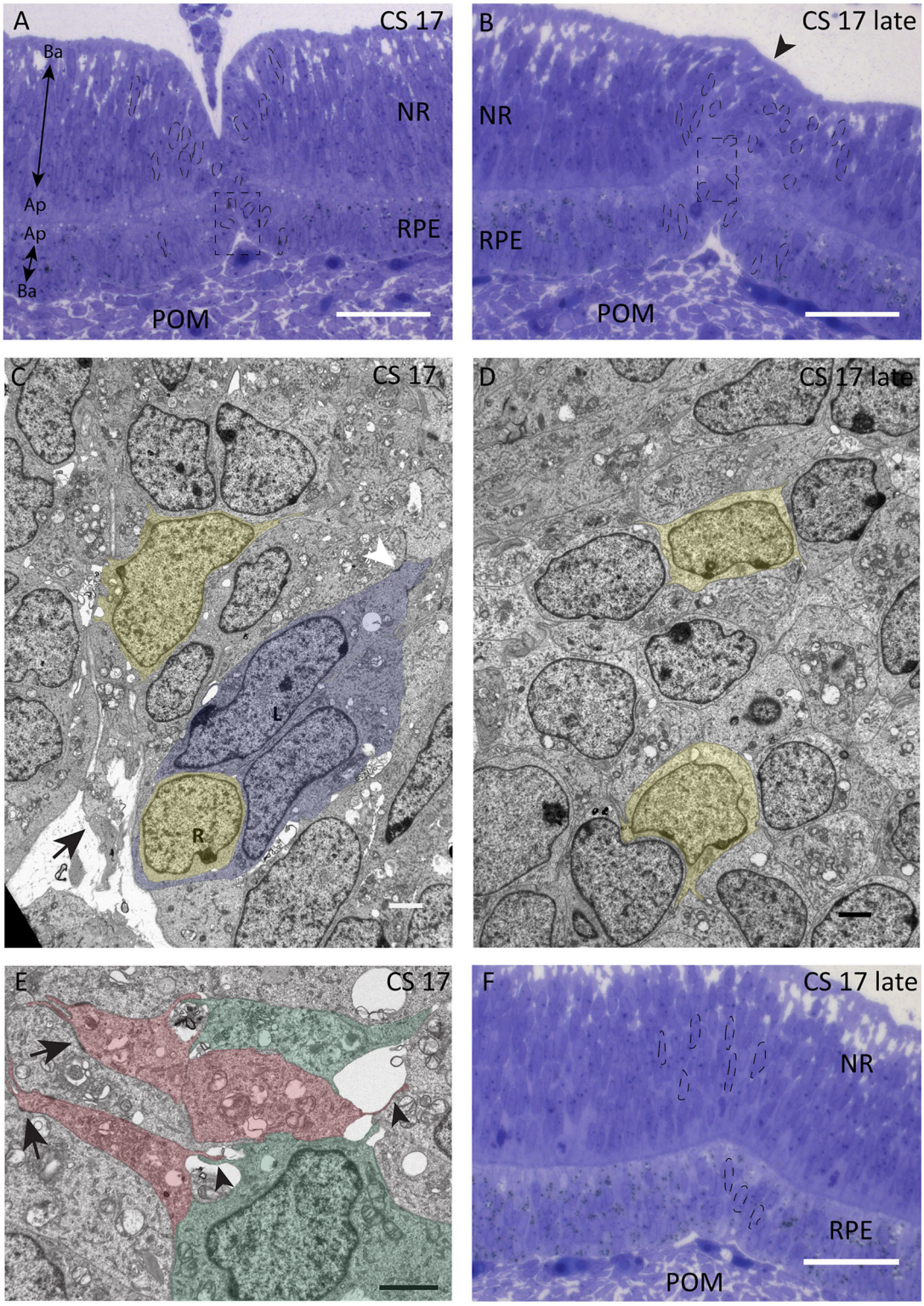

Fig. 5. Electron microscopy of human optic fissure. (A,B) Semi-thin Toluidine Blue stained histological human eye sections during OFC show cells of NR and RPE with a typical epithelial arrangement and elongated nuclei. At the point of closure (B, arrowhead), the cells form a more disorganised group with a rounded nuclear morphology; selected nuclei are outlined in black. (C) Electron micrograph of boxed region from A, showing cells beginning to lose their columnar epithelial morphology. Some cells have adopted a rounded morphology (yellow), whereas others still have an elongated shape (blue) with junctions at their apical ends (white arrowhead). Cellular material appeared to be extruded from the neuroepithelium (arrow). R and L indicate rounded and elongated cells. (D) Electron micrograph of boxed region from B, showing cells with a rounded morphology (yellow) and lacking epithelial organisation. (E) Cells at the fissure margins extend cytoplasmic processes from their basal ends (arrowheads) while maintaining cell junctions with neighbouring neuroepithelial cells at their apical ends (arrows). Red and green indicate cells from opposing sides of the fissure margin (boxed region in Fig. S6B). (F) Semi-thin Toluidine Blue stained histological section of the closed fissure margin region shows cells of the NR and RPE with a typical epithelial arrangement and elongated nuclei. Ap, apical; Ba, basal; POM, periocular mesenchyme; RPE, retinal pigmented epithelium; NR, neural retina. Scale bars: 50 µm in A,B,F; 2 µm in C-E.

Development (2020) 147, dev193649. doi:10.1242/dev.193649

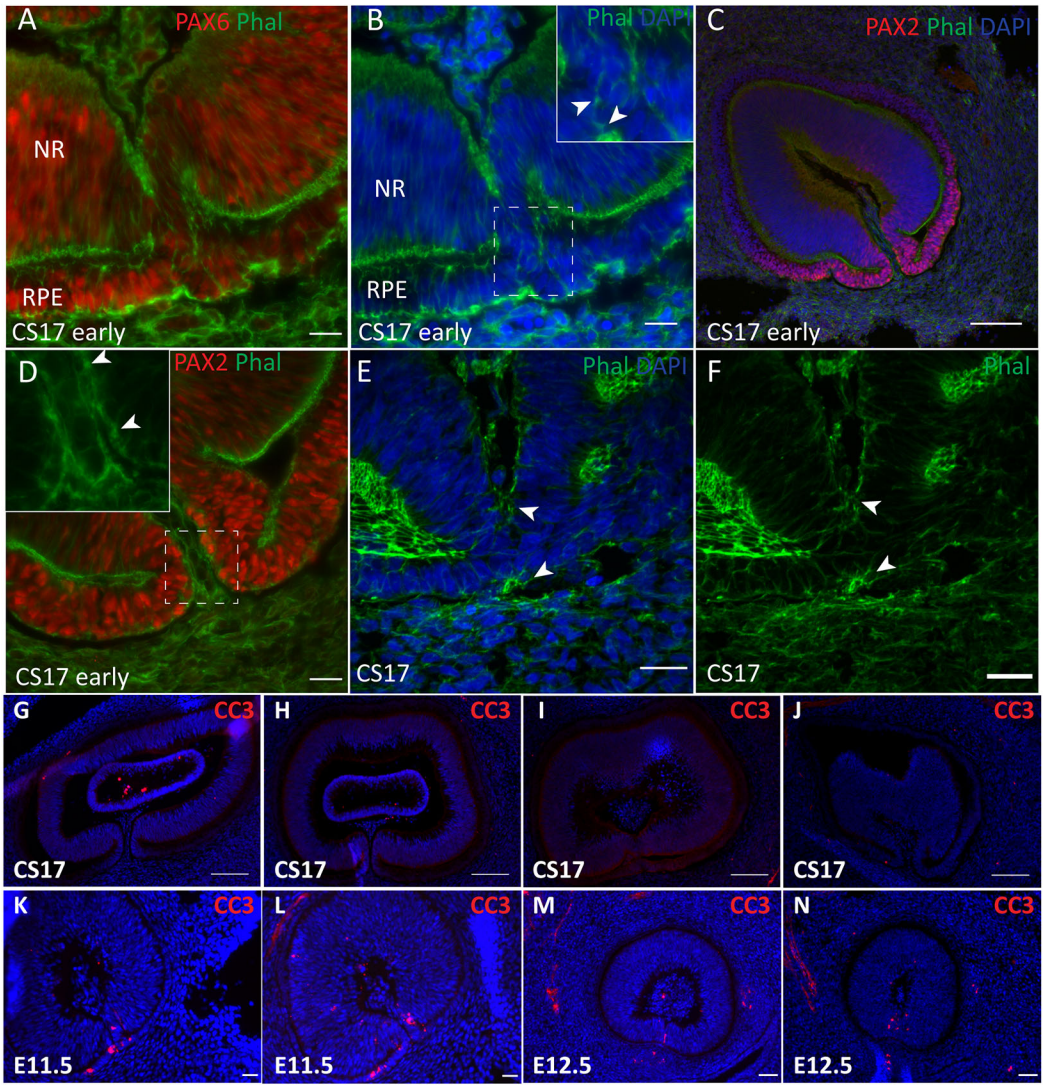

Fig. 6. Staining for filamentous actin and cleaved caspase 3 in cells of the fissure margins. (A-F) Phalloidin staining for filamentous actin. Actin-rich foci (phalloidin; green) were observed: among the rearranging cells at the point of closure (B, inset, arrowheads); in the posterior optic cup in the cells lining the fissure margins (D, inset, arrowheads); and in the group of rearranging cells at the point of closure (E,F, arrowheads). Cells at the fissure margins were counterstained for PAX6, a marker of neuroepithelium of the optic cup (A), or for PAX2, a marker of posterior optic fissure margins (C,D), to differentiate them from the surrounding POM. See also Fig. S6 and Movies 1-4 showing 3D projections of phalloidin staining with DAPI, PAX6 and WGA. (G-N) Immunolabelling for cleaved caspase 3 (CC3, red) on human and mouse eyes. Apoptotic cells were not observed in the human optic fissure margins; a few were present in the developing lens (G-J). Apoptotic cells were observed in the mouse optic fissure margins at E11.5 and at E12.5 (K-N). Scale bars: 20 µm in A,B,D-F; 100 µm in C,G-J; 20 µm in K,L; 50 µm in M,N.

(Yan et al., 2014; Lee et al., 2014). Both EMT and NF-κB gene sets were positively correlated with the OFC in our data.

The change in cell state at the OFMs is likely transient and reversible

Enrichment at the fissure of the EMT gene set (and related gene sets MTORC signalling and NF-κB signalling) was seen in the human and in the mouse at E11.5. By contrast, at E12.5 this gene set was strongly negatively correlated with the fissure margins. Histological and ultrastructural analysis showed a group of cells at the OFMs that did not have an epithelial morphology or arrangement at the closure point, whereas parallel sections (closer to the point of initiation) containing already closed fissure did not show this group of reorganising cells. Instead, the epithelium of the fused margins appeared indistinguishable from the adjacent neural retina. Although cells at the OFMs showed phalloidin staining characteristic of cell protrusions, lost ZO-1 and expressed vimentin, they did not lose expression of *PAX6*, a marker of neuroepithelium in the optic cup. Thus, EMT followed by mesenchymal-epithelial transition (MET) appears to underlie human OFC. This is consistent with the current understanding that cells can be plastic and move between epithelial and mesenchymal states during embryogenesis in multiple organs (Nieto, 2013; Thiery et al., 2009). Consistent with our observations, a recent study comparing the mouse fissure margin with nasal and temporal optic cup transcriptomes at E11.5 showed that the GO BP term ‘positive regulation of cell migration’ and GO MF terms related to ECM binding were strongly enriched in the fissure margin gene set (Cao et al., 2018b).

The change in cell morphology is conserved across species

Extension of cellular protrusions were described in the mouse optic fissure (Hero, 1990) by TEM and a transient loss of epithelial morphology has been observed in the zebrafish eye (Gestri et al.,

Development (2020) 147, dev193649. doi:10.1242/dev.193649

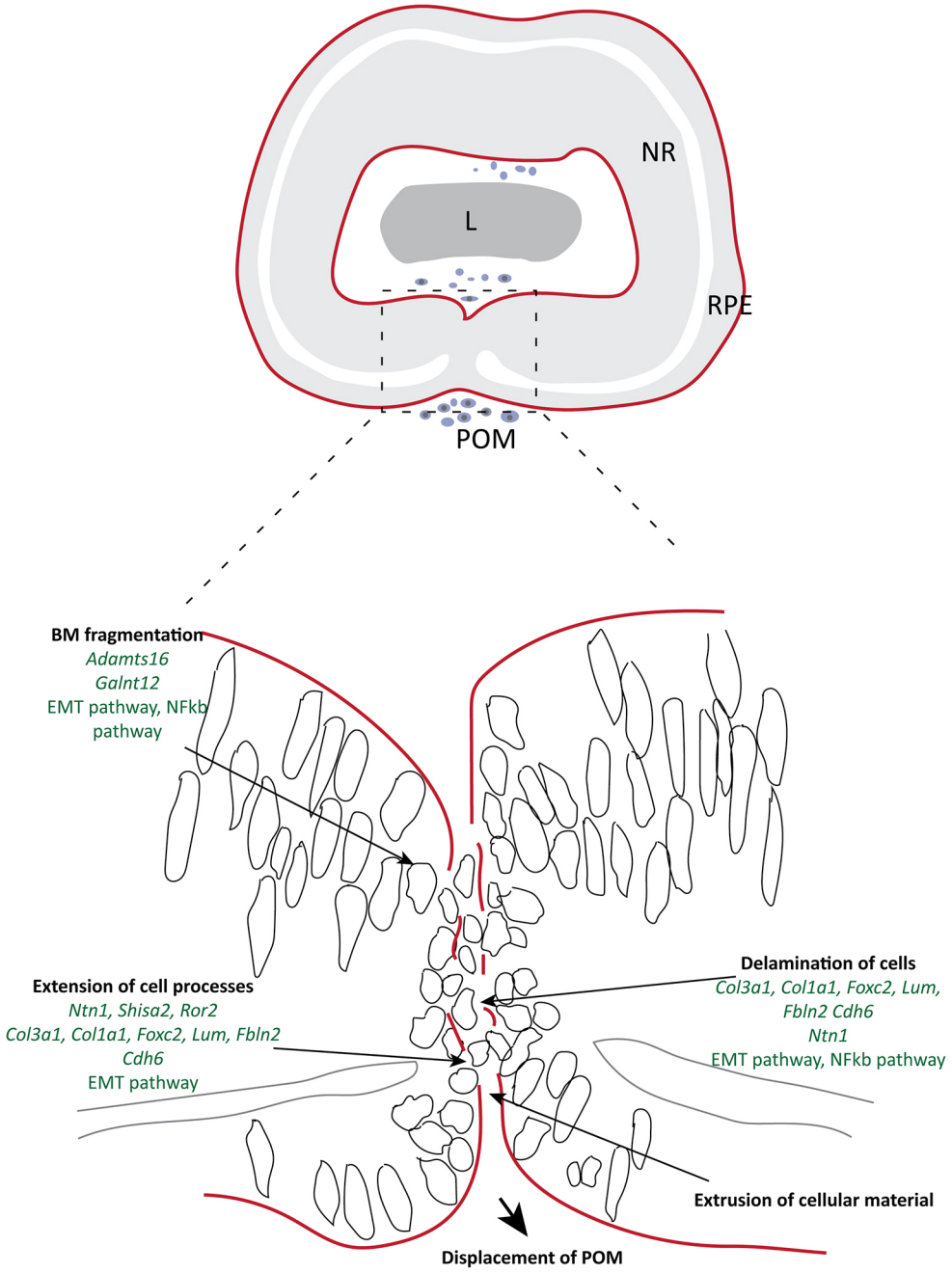

Fig. 7. Schematic representation of cell behaviour and candidate genes at the human OFMs. As OFMs approach each other, intervening POM cells are displaced, the basement membrane fragments, and cells extend processes and undergo a change in cell state and organisation similar to a partial epithelial-to-mesenchymal transition. Candidate genes and gene sets identified in the OFC transcriptome analysis that may be involved in these processes are indicated.

2018). A recent morphological study in the chick eye showed a group of cells delaminating from the optic fissure margins and occupying the space in between (Bernstein et al., 2018). However, there is limited evidence of the molecular regulators of this change.

Change in state of fissure margin cells may be facilitated by changes in ECM composition

Change in ECM properties, including increases in matrix stiffness, are known to facilitate changes in cell state (Greenburg and Hay, 1988), and can result from changes in matrix components secreted by cells and the secretion of extracellular enzymes. In a recent zebrafish study morpholino knockdown of Adamts16 resulted in coloboma with a failure in basement membrane breakdown (Cao et al., 2018a). We show that expression of the human orthologue *ADAMTS16* (a matrix metalloproteinase; Apte, 2009) was enriched in human OFMs at CS17 (FC=10.348, P_{adj}=0.003). EMT is known to involve a change in the collagens secreted into the matrix (Gonzalez and Medici, 2014). We found dynamic regulation of a number of collagen genes in human and mouse at the fissure margins. Lumican is another secreted protein component of the ECM that was enriched at the fissure margins and downregulated over time in the mouse. LUM is involved in collagen fibril assembly and EMT following injury in corneal and lens epithelial cells (Nikitovic et al., 2008; Saika et al., 2003; Chakravarti et al., 2000).

Study limitations

We used laser capture micro-dissection to collect the entire length of the OFMs, including open, closing and closed regions. RNAseq analyses of microdissected regions from three embryos may have detected only a fraction of the genes that are differentially expressed during the dynamic OFC period. Sample variability may have led to genes that are differentially expressed transiently, or in a small

Development (2020) 147, dev193649. doi:10.1242/dev.193649

number of cells, not crossing the significance threshold. If different mechanisms of closure predominate in the distal and proximal regions, such as has been suggested in the chick (Bernstein et al., 2018), this would likely be missed. As we compared gene expression across different regions of the optic cup, it is also likely that a subset of the genes we identified are players in retino-tectal mapping (Torborg and Feller, 2005). Nevertheless we found 22% of genes passing the significance thresholds in the human OF analysis showed conserved expression in the mouse OF analysis. The two species may use different mechanisms of epithelial fusion at the fissure, or use different gene regulatory pathways to achieve the same cellular changes; however, this seems unlikely as we found that key disease genes showed conserved patterns of expression. Our histological analysis confirmed active points of closure at these stages of human development. Owing to the rarity and variable quality of human embryonic tissue the number of biological replicates available for OFC analysis was limited. In future work, scRNAseq analysis may help to further elucidate different molecular cell profiles.

MATERIALS AND METHODS

Embryonic eye samples

Human embryonic eyes were obtained from the Joint Medical Research Council UK (grant G0700089)/Wellcome Trust (grant GR082557) Human Developmental Biology Resource (http://www.hdbr.org/) with ethics approval. Samples at Carnegie Stage (CS) 15, 16, 17 and 18 were analysed. The Carnegie staging system was used to determine the age of embryo as days post ovulation based on morphological landmarks (O'Rahilly and Muller, 1987): CS15, day 33 (7-9 mm crown rump length); CS16, day 37 (11-14 mm); CS17, day 41 (11-14 mm); CS19, day 44 (13-17 mm). C57Bl6 mice were used for comparative studies of the normal mouse optic fissure. Timed matings were set up overnight and midday on the day of identifying a positive vaginal plug was considered as embryonic day 0.5. At embryonic days (E) 11.5 and 12.5, pregnant female mice were sacrificed by CO_2 inhalation followed by cervical dislocation. The uterus was removed and transferred to ice-cold PBS (phosphate-buffered saline, Oxoid BR0014G) and kept on ice before dissection.

Histology

For histology, dissected tissue was fixed in 4% w/v PFA overnight, washed in PBS (3×10 min) and dehydrated in a graded series of ethanol (Hayman) at 4°C, cleared with chloroform at room temperature, followed by incubation in paraffin at 60°C and embedded in paraffin blocks. Paraffin sections were prepared in the parasagittal plane at a thickness of 8 µm; serial sections of the eye in the plane perpendicular to the optic fissure were used to examine the process of OFC. Sections were cleared with Histo-Clear II reagent (National Diagnostics) and rehydrated with graded ethanol series (100%, 95% and 70%). Sections were then stained with Harris Haematoxylin solution (Sigma-Aldrich) for 1 min and with 1% Eosin (Sigma-Aldrich) solution for 2 min with repeated washes in distilled water. The sections were dehydrated in graded ethanol series cleared in Histo-Clear reagent II (National Diagnostics) followed by mounting with DPX mountant (Sigma-Aldrich).

Immunohistochemistry

For immunohistochemistry, dissected tissue was fixed in 4% w/v PFA for 1 h, washed in PBS (3×10 min), equilibrated in 30% w/v sucrose embedded in OCT medium (VWR) and snap frozen in dry ice. The frozen blocks were sectioned at 10-12 µm in the para-sagittal plane. Frozen sections were thawed and the embedding matrix was cleared with PBS at 37°C for 10 min. They were then treated with blocking solution 10% foetal bovine serum or goat serum, 1% bovine serum albumin (Sigma-Aldrich) and 0.1% Triton-X100 in PBS, for 1 h at room temperature. Primary antibody, diluted in the blocking solution, was applied overnight at 4°C (anti-laminin, 1:200, Sigma-Aldrich L9393; anti-Vim, 1:800, Dako MO725; anti-ZO-1, 1:300, Life Technologies, 402200; anti-PAX6, 1:1000, Covance-Biolegend 901301; anti-Pax2, 1:300, Biolegend 901001) Slides were washed in PBS (3×5 min). The secondary antibody (Alexa Fluor 594 goat anti-rabbit IgG or Alexa Fluor 488 donkey anti-sheep IgG) diluted 1:800 in the blocking solution was applied for 1 h at room temperature, followed by Alexa Fluor 488-conjugated phalloidin, Alexa Fluor 647-conjugated wheat germ agglutinin (WGA) and/or DAPI (4′,6-diamidino-2-phenylindole, Sigma-Aldrich) in PBS for 10 min and washing in PBS (3×10 min). The slides were mounted using Hydromount (National Diagnostics HS-106) reagent and stored at −20°C.

Microscopy and image analysis

Fluorescence imaging was performed using a Zeiss Observer microscope with four colour fluorescence or spinning disk confocal microscope (Yokogawa, CSU22). Image analysis was carried out using Fiji/ImageJ. *Z*-stacks were deconvolved using five iterations of the Richardson-Lucy algorithm in DeconvolutionLab2 (Sage et al., 2017). Cell outlines were manually annotated and roundness was measured using in-built plug-ins in Fiji. Roundness heatmaps were generated by multiplying the roundness value of each cell (range 0 to 1) by 255 to derive an 8-bit colour attribution that was then applied to its pre-saved ROI. Heatmaps are displayed using Fire LUT.

Electron microscopy

Samples were fixed in 2.5% glutaraldehyde buffered in 0.1 M sodium cacodylate (pH 7.2), post-fixed in 1% osmium tetroxide and then dehydrated in ascending grades of ethanol. Tissue blocks were passed through a transitional fluid, propylene oxide, and then infiltrated overnight in Epon resin. The blocks were then transferred to BEEM capsules with fresh resin and polymerised at 60°C for 48 h. Ultrathin sections were cut with a Diatome diamond knife at 90 nm on a Leica Ultracut UCT ultramicrotome, placed on copper grids and stained with uranyl acetate and lead citrate. Examination was carried out using a JEOL 1400 transmission electron microscope and images recorded using an AMT XR80 digital camera.

RNAseq

Human embryonic eyes at CS17 and CS18 were dissected, and the eye along with surrounding periocular mesenchyme were embedded in OCT medium (VWR) and snap frozen on dry ice. C57Bl6 mouse embryos were collected at E11.5 and E12.5. The embryos were dissected in PBS and heads were dissected, followed by embedding in OCT medium (VWR), snap freezing on dry ice and storage at −80°C prior to sectioning. The blocks were stored at −80°C.

The embedded eyes (in the case of human embryos) or heads (in the case of mouse embryos) were sectioned in the parasagittal plane, i.e. perpendicular to the optic fissure at a thickness of 20 µm at −20°C and the sections were collected on PEN (polyethylene naphthalate) membrane-coated slides (Thermo Fisher LCM0522). Slides with sections were stored at −80°C. Slides were thawed, air dried and viewed under bright-field illumination on a laser capture microdissection microscope (PALM microbeam). The eye was orientated and optic fissure identified. The region of interest containing the fissure margins and excluding the periocular mesenchyme and lens was identified and outlined using the graphic tool of the PALM Robo software, cut out using a UV laser and catapulted with the laser into the cap of a collection tube (Zeiss, 415190-9211-000). Fissure margin regions were collected along the length of the fissure, beginning with the first section in which both margins could be clearly visualised and ending with the last section before the optic nerve head became visible. In case a section was damaged and the fissure could not be clearly identified, no tissue was collected from it. The fissure margins of the two eyes of each embryo were pooled in the same collection tube. Similarly, a control region was cut out of the dorsal optic cup and pooled using a fresh collection tube. Lysis buffer (Qiagen RNeasy Micro kit, 74004) was added to the collection tube, the caps were closed and the tube was inverted vigorously several times to rapidly lyse the tissue and prevent RNA degradation. The tube was immediately frozen on dry ice and stored at −80°C. Total RNA was extracted using standard protocols, and treated with DNAseI (Qiagen). RNA quality and concentration were determined using

Development (2020) 147, dev193649. doi:10.1242/dev.193649

the Tapestation (Agilent Technologies). Only RNA samples with intact 18S and 28S bands were used for sequencing. Approximately 1.2 and 10 ng RNA was isolated per human and mouse embryo, respectively, for analysis of the fissure margin and dorsal region by RNAseq. RNA samples were amplified and cDNA libraries prepared using the SMART-Seq v4 Ultra Low Input RNA (Clontech Laboratories) and Nextera XT DNA Library Preparation (Illumina) kits, and cDNA quality was assessed using Qubit dsDNA HS Assay kit and Qubit 2.0 Fluorometer (ThermoFisher). cDNA libraries were sequenced in four lanes on the Illumina NextSeq500 platform using 43 bp paired end reads. Fissure margin and dorsal retina samples of replicate embryos within each development time point were sequenced within the same run. Sequencing yielded an average of 19 million reads (range: 13-24 million) per mouse sample and 27 million (range: 23-33 million) reads per human sample.

Bioinformatics

Following quality control, sequencing reads (FastQ) of cDNA libraries were aligned, using the Illumina RNA Seq STAR alignment tool (version 1.1.0) to the relevant reference genome (human, GRCh37/hg19; mouse, GRCm38/m10), followed by post-alignment QC. The majority of reads aligned to coding or untranslated (UTR) regions as expected (Fig. S3B,C). Further analysis was carried out in the R programming environment (version 3.3.2). Aligned reads were assigned to genes and quantified using featureCounts (Rsubread package v. 1.24.1) (Liao et al., 2014). Genes were pre-filtered based on raw counts, retaining genes that had a total of at least five reads across all samples in one analysis. Normalisation and principal component analysis was carried out using the DESeq2 (v. 1.14.1) (Love et al., 2015). A global principal component analysis (PCA) using the normalised counts showed that the human fissure margin and dorsal samples separated from each other along the first principal component of the PCA plot. Two fissure margin samples at CS17 clustered closely together, and one CS17 dorsal sample [CS17(2) D] was outlying (which may be explained by QC indicating limited 3′-bias due to degradation; Fig. S3B). The fissure margins and dorsal optic cup samples at E11.5 and E12.5, from the mouse eye also separated from each other along the first principal component of the PCA plot. (Fig. S3E). Heatmaps of normalised read counts were plotted using the pheatmap package (version 1.0.8).

Differential gene expression analysis used the DESeq2 package (v. 1.14.1). In the case of the human samples, a modification of the DESeq2 algorithm for paired analysis was used to account for the greater variability of the samples and the smaller number of replicates. A significance threshold of adjusted *P*-value threshold <0.05 and a $\log_2$ fold change threshold of >1 (referred to as fissure-enriched genes) or <−1 (referred to as dorsal-enriched genes) (i.e. fold change >2 or <0.5) was applied to identify significantly differentially expressed genes. Differential expression analysis was carried out for fissure margin samples versus dorsal control samples within each time point and fissure margin samples between the two time points. Volcano plots were plotted using $\log_2$ fold changes and adjusted *P*-values. Gene ontology enrichment analysis was used to annotate the significantly differentially expressed genes using the gene ontology database (http://amigo.geneontology.org/amigo/landing). A list consisting of the significantly fissure-enriched and dorsal-enriched genes from each dataset was analysed using the DAVID enrichment tool (https://david.ncifcrf.gov/summary.jsp) and the species-relevant background. The RNAseq datasets were also analysed for differential expression at the level of gene sets. Genes were ranked by $\log_2$ fold change calculated using DESeq2, as described above. Mouse genes were converted into their human orthologues using web-based dbOrtho tool at BiodbNet (https://biodbnet-abcc.ncifcrf.gov/ and https://www.ncbi.nlm.nih.gov/gene). The list was imported into gene set enrichment software (GSEA 3.0) (Subramanian et al., 2005). GSEA evaluates small changes in a large number of genes that together may significantly influence a pathway or cell mechanism, and provides biologically meaningful results that complement simple differential expression analysis. A pre-ranked analysis was run using the 50 hallmark curated gene sets from the molecular signature database (Liberzon et al., 2015) and a false discovery rate threshold of FDR<0.25 (Subramanian et al., 2005). RNAseq data have been deposited in ArrayExpress under accession numbers E-MTAB-9426 and E-MTAB-9427.

qRT PCR

Expression of selected genes in microdissected tissue was verified using qRT PCR. 1 ng of total RNA, treated with DNAase1 (Qiagen), was used as a template to synthesise cDNA (RevertAid H Minus First Strand cDNA Synthesis Kit, K1631). cDNA samples were diluted to the same concentration (0.5 ng/µl) with nuclease-free water. The qRT PCR procedure was carried out in 96-well plates with a total reaction volume of 20 µl per well [10 µl Power SYBR Green Master Mix, 1 µl gene specific primers (10 µm), 1 µl cDNA, 8 µl nuclease-free water]. Primers used were as follows: ALDH1A3, 5′TGAATGGCACGAATCCAAGAG3′ and 5′CACGTCGGGCTTATCTCCT3′; SMOC1, 5′AGGTCCTACGAGTCCATGTGT3′ and 5′CACTGCACCTGGGTAAAGG3′; ATP1A2, 5′GGCCGCAAATACCAAGTGGA3′ and 5′CCACACCCAGATATAGATTGTCG3′; TENM3, 5′AAGCAGACGAGTTCACTAGACA3′ and 5′TCCTCTTCGAGTTGCTGGTTC3′; TBX5, 5′CTGTGGCTAAAATTCCACGAAGT3′ and 5′GTGATCGTCGGCAGGTACAAT3′. The following PCR cycle was used for all samples: 95°C for 10 min, 40 cycles of 95°C for 15 s and 60°C for 1 min. Ct values were normalised against results for Actin (primers 5′ATAGCAACGTACATGGCTGG3′ and 5′CACCTCTACAATGAGCTGC3′).

Acknowledgements

The views expressed are those of the authors and not necessarily those of the NHS, the NIHR or the Department of Health. The human embryonic and foetal material was provided by the Joint MRC/Wellcome Trust Human Developmental Biology Resource (www.hdbr.org). We thank Dale Moulding at the Imaging Facility UCL GOS ICH and Tony Brooks at UCL Genomics for technical support, the UCL Institute of Ophthalmology for use of the Laser Capture microscope, Joe Rainger and Daniel Holder for comments on the manuscript, and all staff in the Human Developmental Biology Resource.

Competing interests

The authors declare no competing or financial interests.

Author contributions

Conceptualization: A.P., J.C.S.; Methodology: A.P., G.A., G.G., M.B.; Validation: A.P.; Formal analysis: A.P., J.C.S; Investigation: A.P., G.A., G.G., M.B.; Writing - original draft: A.P., J.C.S.; Writing - review & editing: A.P., J.C.S.; Supervision: J.C.S.; Funding acquisition: J.C.S.

Funding

This work was supported by the National Institute for Health Research Great Ormond Street Hospital Biomedical Research Centre and the Rosetrees Trust. A.P. was funded by the University College London Graduate Research and Overseas Research Scholarships, and by the National Institute for Health Research Great Ormond Street Hospital BRC Doctoral Training Support Fund. J.C.S. is funded by the Great Ormond Street Hospital Children's Charity and by the Medical Research Council (MR/S036237/1).

Data availability

RNAseq data have been deposited in ArrayExpress under accession numbers E-MTAB-9426 and E-MTAB-9427.

Supplementary information

Supplementary information available online at
https://dev.biologists.org/lookup/doi/10.1242/dev.193649.supplemental

References

Apte, S. S. (2009). A disintegrin-like and metalloprotease (reprolysin-type) with thrombospondin type 1 motif (ADAMTS) superfamily: functions and mechanisms. *J. Biol. Chem.* **284**, 31493-31497. doi:10.1074/jbc.R109.052340

Babb, S. G., Kotradi, S. M., Shah, B., Chiappini-Williamson, C., Bell, L. N., Schmeiser, G., Chen, E., Liu, Q. and Marrs, J. A. (2005). Zebrafish R-cadherin (Cdh4) controls visual system development and differentiation. *Dev. Dyn.* **233**, 930-945. doi:10.1002/dvdy.20431

Barbieri, A. M., Lupo, G., Bulfone, A., Andreazzoli, M., Mariani, M., Fougerousse, F., Consalez, G. G., Borsani, G., Beckmann, J. S., Barsacchi, G. et al. (1999). A homeobox gene, vax2, controls the patterning of the eye dorsoventral axis. *Proc. Natl. Acad. Sci. USA* **96**, 10729-10734. doi:10.1073/pnas.96.19.10729

Barbieri, A. M., Broccoli, V., Bovolenta, P., Alfano, G., Marchitiello, A., Mocchetti, C., Crippa, L., Bulfone, A., Marigo, V., Ballabio, A. et al. (2002). Vax2 inactivation in mouse determines alteration of the eye dorsal-ventral axis, misrouting of the optic fibres and eye coloboma. *Development* **129**, 805-813.

Behesti, H., Holt, J. K. L. and Sowden, J. C. (2006). The level of BMP4 signaling is critical for the regulation of distinct T-box gene expression domains and growth along the dorso-ventral axis of the optic cup. *BMC Dev. Biol.* **6**, 62. doi:10.1186/1471-213X-6-62

Behesti, H., Papaioannou, V. E. and Sowden, J. C. (2009). Loss of Tbx2 delays optic vesicle invagination leading to small optic cups. *Dev. Biol.* **333**, 360-372. doi:10.1016/j.ydbio.2009.06.026

Bernstein, C. S., Anderson, M. T., Gohel, C., Slater, K., Gross, J. M. and Agarwala, S. (2018). The cellular bases of choroid fissure formation and closure. *Dev. Biol.* **440**, 137-151. doi:10.1016/j.ydbio.2018.05.010

Bogdanović, O., Delfino-Machín, M., Nicolás-Pérez, M., Gavilán, M. P., Gago-Rodrigues, I., Fernández-Miñán, A., Lillo, C., Ríos, R. M., Wittbrodt, J. and Martínez-Morales, J. R. (2012). Numb/Numbl-Opo antagonism controls retinal epithelium morphogenesis by regulating integrin endocytosis. *Dev. Cell* **23**, 782-795. doi:10.1016/j.devcel.2012.09.004

Brown, J. D., Dutta, S., Bharti, K., Bonner, R. F., Munson, P. J., Dawid, I. B., Akhtar, A. L., Onojafe, I. F., Alur, R. P., Gross, J. M. et al. (2009). Expression profiling during ocular development identifies 2 Nlz genes with a critical role in optic fissure closure. *Proc. Natl. Acad. Sci. USA* **106**, 1462-1467. doi:10.1073/pnas.0812017106

Byström, B., Virtanen, I., Rousselle, P., Gullberg, D. and Pedrosa-Domellöf, F. (2006). Distribution of laminins in the developing human eye. *Invest. Ophthalmol. Vis. Sci.* **47**, 777-785. doi:10.1167/iovs.05-0367

Cao, M., Ouyang, J., Guo, J., Lin, S. and Chen, S. (2018a). Metalloproteinase adamts16 is required for proper closure of the optic fissure. *Invest. Ophthalmol. Vis. Sci.* **59**, 1167-1177. doi:10.1167/iovs.17-22827

Cao, M., Ouyang, J., Liang, H., Guo, J., Lin, S., Yang, S., Xie, T. and Chen, S. (2018b). Regional gene expression profile comparison reveals the unique transcriptome of the optic fissure. *Invest. Ophthalmol. Vis. Sci.* **59**, 5773-5784. doi:10.1167/iovs.18-23962

Chakravarti, S., Petroll, W. M., Hassell, J. R., Jester, J. V., Lass, J. H., Paul, J. and Birk, D. E. (2000). Corneal opacity in lumican-null mice: defects in collagen fibril structure and packing in the posterior stroma. *Invest. Ophthalmol. Vis. Sci.* **41**, 3365-3373.

Chen, S., Lewis, B., Moran, A. and Xie, T. (2012). Cadherin-mediated cell adhesion is critical for the closing of the mouse optic fissure. *PLoS ONE* **7**, e51705. doi:10.1371/journal.pone.0051705

Chen, Y., Londraville, R., Brickner, S., El-Shaar, L., Fankhauser, K., Dearth, C., Fulton, L., Sochacka, A., Bhattarai, S., Marrs, J. A. and Liu, Q. (2013). Protocadherin-17 function in zebrafish retinal development. *Dev. Neurobiol.* **73**, 259-273. doi:10.1002/dneu.22053

Chiang, C., Litingtung, Y., Lee, E., Young, K. E., Corden, J. L., Westphal, H. and Beachy, P. A. (1996). Cyclopia and defective axial patterning in mice lacking Sonic hedgehog gene function. *Nature* **383**, 407-413. doi:10.1038/383407a0

Chou, C. M., Nelson, C., Tarlé, S. A., Pribila, J. T., Bardakjian, T., Woods, S., Schneider, A. and Glaser, T. (2015). Biochemical basis for dominant inheritance, variable penetrance, and maternal effects in RBP4 congenital eye disease. *Cell* **161**, 634-646. doi:10.1016/j.cell.2015.03.006

Chua, H. L., Bhat-Nakshatri, P., Clare, S. E., Morimiya, A., Badve, S. and Nakshatri, H. (2007). NF-kappaB represses E-cadherin expression and enhances epithelial to mesenchymal transition of mammary epithelial cells: potential involvement of ZEB-1 and ZEB-2. *Oncogene* **26**, 711-724. doi:10.1038/sj.onc.1209808

Deiner, M. S., Kennedy, T. E., Fazeli, A., Serafini, T., Tessier-Lavigne, M. and Sretavan, D. W. (1997). Netrin-1 and DCC mediate axon guidance locally at the optic disc: loss of function leads to optic nerve hypoplasia. *Neuron* **19**, 575-589. doi:10.1016/S0896-6273(00)80373-6

Dudas, M., Li, W.-Y., Kim, J., Yang, A. and Kaartinen, V. (2007). Palatal fusion - where do the midline cells go? A review on cleft palate, a major human birth defect. *Acta Histochem.* **109**, 1-14. doi:10.1016/j.acthis.2006.05.009

Dupe, V., Matt, N., Garnier, J.-M., Chambon, P., Mark, M. and Ghyselinck, N. B. (2003). A newborn lethal defect due to inactivation of retinaldehyde dehydrogenase type 3 is prevented by maternal retinoic acid treatment. *Proc. Natl. Acad. Sci. USA* **100**, 14036-14041. doi:10.1073/pnas.2336223100

Echelard, Y., Epstein, D. J., St-Jacques, B., Shen, L., Mohler, J., Mcmahon, J. A. and Mcmahon, A. P. (1993). Sonic hedgehog, a member of a family of putative signaling molecules, is implicated in the regulation of CNS polarity. *Cell* **75**, 1417-1430. doi:10.1016/0092-8674(93)90627-3

Ekblom, P., Ekblom, M., Fecker, L., Klein, G., Zhang, H. Y., Kadoya, Y., Chu, M. L., Mayer, U. and Timpl, R. (1994). Role of mesenchymal nidogen for epithelial morphogenesis in vitro. *Development* **120**, 2003-2014.

Fekete, D. M., Homburger, S. A., Waring, M. T., Riedl, A. E. and Garcia, L. F. (1997). Involvement of programmed cell death in morphogenesis of the vertebrate inner ear. *Development* **124**, 2451-2461.

Franke, W. W., Grund, C., Kuhn, C., Jackson, B. W. and Illmensee, K. (1982). Formation of cytoskeletal elements during mouse embryogenesis. III. Primary mesenchymal cells and the first appearance of vimentin filaments. *Differentiation* **23**, 43-59. doi:10.1111/j.1432-0436.1982.tb01266.x

Fuhrmann, S. (2010). Eye morphogenesis and patterning of the optic vesicle. *Curr. Top. Dev. Biol.* **93**, 61-84. doi:10.1016/B978-0-12-385044-7.00003-5

Gago-Rodrigues, I., Fernández-Miñán, A., Letelier, J., Naranjo, S., Tena, J. J., Gómez-Skarmeta, J. L. and Martinez-Morales, J. R. (2015). Analysis of opo cis-regulatory landscape uncovers Vsx2 requirement in early eye morphogenesis. *Nat. Commun.* **6**, 7054. doi:10.1038/ncomms8054

Gestri, G., Bazin-Lopez, N., Scholes, C. and Wilson, S. W. (2018). Cell behaviors during closure of the choroid fissure in the developing eye. *Front. Cell Neurosci.* **12**, 42. doi:10.3389/fncel.2018.00042

Gonzalez, D. M. and Medici, D. (2014). Signaling mechanisms of the epithelial-mesenchymal transition. *Sci. Signal.* **7**, re8. doi:10.1126/scisignal.2005189

Greenburg, G. and Hay, E. D. (1988). Cytoskeleton and thyroglobulin expression change during transformation of thyroid epithelium to mesenchyme-like cells. *Development* **102**, 605-622.

Hardy, H., Prendergast, J. G. D., Patel, A., Dutta, S., Trejo-Reveles, V., Kroeger, H., Yung, A. R., Goodrich, L. V., Brooks, B., Sowden, J. C. et al. (2019). Detailed analysis of chick optic fissure closure reveals Netrin-1 as an essential mediator of epithelial fusion. *eLife* **8**, e43877. doi:10.7554/eLife.43877

Heermann, S., Schütz, L., Lemke, S., Krieglstein, K. and Wittbrodt, J. (2015). Eye morphogenesis driven by epithelial flow into the optic cup facilitated by modulation of bone morphogenetic protein. *eLife* **4**, e05216. doi:10.7554/eLife.05216

Hero, I. (1990). Optic fissure closure in the normal cinnamon mouse. An ultrastructural study. *Invest. Ophthalmol. Vis. Sci.* **31**, 197-216.

Hero, I., Farjah, M. and Scholtz, C. L. (1991). The prenatal development of the optic fissure in colobomatous microphthalmia. *Invest. Ophthalmol. Vis. Sci.* **32**, 2622-2635.

Hirai, Y., Takebe, K., Takashina, M., Kobayashi, S. and Takeichi, M. (1992). Epimorphin: a mesenchymal protein essential for epithelial morphogenesis. *Cell* **69**, 471-481. doi:10.1016/0092-8674(92)90448-L

Jacinto, A., Wood, W., Balayo, T., Turmaine, M., Martinez-Arias, A. and Martin, P. (2000). Dynamic actin-based epithelial adhesion and cell matching during Drosophila dorsal closure. *Curr. Biol.* **10**, 1420-1426. doi:10.1016/S0960-9822(00)00796-X

James, A., Lee, C., Williams, A. M., Angileri, K., Lathrop, K. L. and Gross, J. M. (2016). The hyaloid vasculature facilitates basement membrane breakdown during choroid fissure closure in the zebrafish eye. *Dev. Biol.* **419**, 262-272. doi:10.1016/j.ydbio.2016.09.008

Kim, T.-H., Goodman, J., Anderson, K. V. and Niswander, L. (2007). Phactr4 regulates neural tube and optic fissure closure by controlling PP1-, Rb-, and E2F1-regulated cell-cycle progression. *Dev. Cell* **13**, 87-102. doi:10.1016/j.devcel.2007.04.018

Kim, S., Lewis, A. E., Singh, V., Ma, X., Adelstein, R. and Bush, J. O. (2015). Convergence and extrusion are required for normal fusion of the mammalian secondary palate. *PLoS Biol.* **13**, e1002122. doi:10.1371/journal.pbio.1002122

Kobayashi, Y., Nakamura, H. and Funahashi, J.-I. (2008). Epithelial-mesenchymal transition as a possible mechanism of semicircular canal morphogenesis in chick inner ear. *Tohoku J. Exp. Med.* **215**, 207-217. doi:10.1620/tjem.215.207

Lamouille, S. and Derynck, R. (2007). Cell size and invasion in TGF-beta-induced epithelial to mesenchymal transition is regulated by activation of the mTOR pathway. *J. Cell Biol.* **178**, 437-451. doi:10.1083/jcb.200611146

Lee, J., Lee, B.-K. and Gross, J. M. (2013). Bcl6a function is required during optic cup formation to prevent p53-dependent apoptosis and colobomata. *Hum. Mol. Genet.* **22**, 3568-3582. doi:10.1093/hmg/ddt211

Lee, S.-J., Jung, Y. H., Oh, S. Y., Yong, M. S., Ryu, J. M. and Han, H. J. (2014). Netrin-1 induces MMP-12-dependent E-cadherin degradation via the distinct activation of PKCα and FAK/Fyn in promoting mesenchymal stem cell motility. *Stem Cells Dev.* **23**, 1870-1882. doi:10.1089/scd.2013.0632

Liao, Y., Smyth, G. K. and Shi, W. (2014). featureCounts: an efficient general purpose program for assigning sequence reads to genomic features. *Bioinformatics* **30**, 923-930. doi:10.1093/bioinformatics/btt656

Liberzon, A., Birger, C., Thorvaldsdóttir, H., Ghandi, M., Mesirov, J. P. and Tamayo, P. (2015). The Molecular Signatures Database (MSigDB) hallmark gene set collection. *Cell Syst.* **1**, 417-425. doi:10.1016/j.cels.2015.12.004

Liu, X., Wu, H., Byrne, M., Krane, S. and Jaenisch, R. (1997). Type III collagen is crucial for collagen I fibrillogenesis and for normal cardiovascular development. *Proc. Natl. Acad. Sci. USA* **94**, 1852-1856. doi:10.1073/pnas.94.5.1852

Liu, Q., Babb, S. G., Novince, Z. M., Doedens, A. L., Marrs, J. and Raymond, P. A. (2001). Differential expression of cadherin-2 and cadherin-4 in the developing and adult zebrafish visual system. *Vis. Neurosci.* **18**, 923-933.

Love, M. I., Anders, S., Kim, V. and Huber, W. (2015). RNA-Seq workflow: gene-level exploratory analysis and differential expression. *F1000Res* **4**, 1070. doi:10.12688/f1000research.7035.1

Masai, I., Lele, Z., Yamaguchi, M., Komori, A., Nakata, A., Nishiwaki, Y., Wada, H., Tanaka, H., Nojima, Y., Hammerschmidt, M. et al. (2003). N-cadherin mediates retinal lamination, maintenance of forebrain compartments and patterning of retinal neurites. *Development* **130**, 2479-2494.

Matt, N., Dupé, V., Garnier, J.-M., Dennefeld, C., Chambon, P., Mark, M. and Ghyselinck, N. B. (2005). Retinoic acid-dependent eye morphogenesis is orchestrated by neural crest cells. *Development* **132**, 4789-4800. doi:10.1242/dev.02031

McLaughlin, M. E., Kruger, G. M., Slocum, K. L., Crowley, D., Michaud, N. A., Huang, J., Magendantz, M. and Jacks, T. (2007). The Nf2 tumor suppressor regulates cell-cell adhesion during tissue fusion. *Proc. Natl. Acad. Sci. USA* **104**, 3261-3266. doi:10.1073/pnas.0700044104

Medici, D. and Nawshad, A. (2010). Type I collagen promotes epithelial-mesenchymal transition through ILK-dependent activation of NF-κB and LEF-1. *Matrix Biol.* **29**, 161-165. doi:10.1016/j.matbio.2009.12.003

Morcillo, J., Martinez-Morales, J. R., Trousse, F., Fermin, Y., Sowden, J. C. and Bovolenta, P. (2006). Proper patterning of the optic fissure requires the sequential activity of BMP7 and SHH. *Development* **133**, 3179-3190. doi:10.1242/dev.02493

Nicholson, D. W., Ali, A., Thornberry, N. A., Vaillancourt, J. P., Ding, C. K., Gallant, M., Gareau, Y., Griffin, P. R., Labelle, M., Lazebnik, Y. A. et al. (1995). Identification and inhibition of the ICE/CED-3 protease necessary for mammalian apoptosis. *Nature* **376**, 37-43. doi:10.1038/376037a0

Nicolás-Pérez, M., Kuchling, F., Letelier, J., Polvillo, R., Wittbrodt, J. and Martinez-Morales, J. R. (2016). Analysis of cellular behavior and cytoskeletal dynamics reveal a constriction mechanism driving optic cup morphogenesis. *eLife* **5**, e15797. doi:10.7554/eLife.15797

Niederreither, K., D'souza, R., Metsäranta, M., Eberspaecher, H., Toman, P. D., Vuorio, E. and DE Crombrugghe, B. (1995). Coordinate patterns of expression of type I and III collagens during mouse development. *Matrix Biol.* **14**, 705-713. doi:10.1016/S0945-053X(05)80013-7

Nieto, M. A. (2013). Epithelial plasticity: a common theme in embryonic and cancer cells. *Science* **342**, 1234850. doi:10.1126/science.1234850

Nikitovic, D., Katonis, P., Tsatsakis, A., Karamanos, N. K. and Tzanakakis, G. N. (2008). Lumican, a small leucine-rich proteoglycan. *IUBMB Life* **60**, 818-823. doi:10.1002/iub.131

Noh, H., Lee, H., Park, E. and Park, S. (2016). Proper closure of the optic fissure requires ephrin A5-EphB2-JNK signaling. *Development* **143**, 461-472. doi:10.1242/dev.129478

Okada, I., Hamanoue, H., Terada, K., Tohma, T., Megarbane, A., Chouery, E., Abou-Ghoch, J., Jalkh, N., Cogulu, O., Ozkinay, F. et al. (2011). SMOC1 is essential for ocular and limb development in humans and mice. *Am. J. Hum. Genet.* **88**, 30-41. doi:10.1016/j.ajhg.2010.11.012

Onwochei, B. C., Simon, J. W., Bateman, J. B., Couture, K. C. and Mir, E. (2000). Ocular colobomata. *Surv. Ophthalmol.* **45**, 175-194. doi:10.1016/S0039-6257(00)00151-X

O'rahilly, R. (1983). The timing and sequence of events in the development of the human eye and ear during the embryonic period proper. *Anat. Embryol.* **168**, 87-99. doi:10.1007/BF00305401

O'rahilly, R. and Muller, F. (1987). *Developmental Stages in Human Embryos: Including a Revision of Streeter's "Horizons" and a Survey of the Carnegie Collection*. Washington, DC: Carnegie Institution of Washington.

Ozeki, H., Ogura, Y., Hirabayashi, Y. and Shimada, S. (2000). Apoptosis is associated with formation and persistence of the embryonic fissure. *Curr. Eye Res.* **20**, 367-372. doi:10.1076/0271-3683(200005)2051-1FT367

Patel, A. and Sowden, J. C. (2017). Genes and pathways in optic fissure closure. *Semin. Cell Dev. Biol.* **91**, 55-65.

Patel, A., Hayward, J. D., Tailor, V., Nyanhete, R., Ahlfors, H., Gabriel, C., Jannini, T. B., Abbou-Rayyah, Y., Henderson, R., Nischal, K. K. et al. (2019). The Oculome panel test: next-generation sequencing to diagnose a diverse range of genetic developmental eye disorders. *Ophthalmology* **126**, 888-907. doi:10.1016/j.ophtha.2018.12.050

Paulson, A. F., Prasad, M. S., Thuringer, A. H. and Manzerra, P. (2014). Regulation of cadherin expression in nervous system development. *Cell Adh. Migr.* **8**, 19-28. doi:10.4161/cam.27839

Reis, L. M. and Semina, E. V. (2015). Conserved genetic pathways associated with microphthalmia, anophthalmia, and coloboma. *Birth Defects Res. C Embryo Today* **105**, 96-113. doi:10.1002/bdrc.21097

Rolo, A., Savery, D., Escuin, S., de Castro, S. C., Armer, H. E. J., Munro, P. M. G., Molè, M. A., Greene, N. D. E. and Copp, A. J. (2016). Regulation of cell protrusions by small GTPases during fusion of the neural folds. *eLife* **5**, e13273. doi:10.7554/eLife.13273

Sage, D., Donati, L., Soulez, F., Fortun, D., Schmit, G., Seitz, A., Guiet, R., Vonesch, C. and Unser, M. (2017). DeconvolutionLab2: An open-source software for deconvolution microscopy. *Methods* **115**, 28-41. doi:10.1016/j.ymeth.2016.12.015

Saika, S., Miyamoto, T., Tanaka, S.-I., Tanaka, T., Ishida, I., Ohnishi, Y., Ooshima, A., Ishiwata, T., Asano, G., Chikama, T.-I. et al. (2003). Response of lens epithelial cells to injury: role of lumican in epithelial-mesenchymal transition. *Invest. Ophthalmol. Vis. Sci.* **44**, 2094-2102. doi:10.1167/iovs.02-1059

See, A. W.-M. and Clagett-Dame, M. (2009). The temporal requirement for vitamin A in the developing eye: mechanism of action in optic fissure closure and new roles for the vitamin in regulating cell proliferation and adhesion in the embryonic retina. *Dev. Biol.* **325**, 94-105. doi:10.1016/j.ydbio.2008.09.030

Shah, S. P., Taylor, A. E., Sowden, J. C., Ragge, N. K., Russell-Eggitt, I., Rahi, J. S., Gilbert, C. E. and **Surveillance of Eye Anomalies Special Interest Group**. (2011). Anophthalmos, microphthalmos, and typical coloboma in the United Kingdom: a prospective study of incidence and risk. *Invest. Ophthalmol. Vis. Sci.* **52**, 558-564. doi:10.1167/iovs.10-5263

Sidhaye, J. and Norden, C. (2017). Concerted action of neuroepithelial basal shrinkage and active epithelial migration ensures efficient optic cup morphogenesis. *eLife* **6**, e22689. doi:10.7554/eLife.22689

Subramanian, A., Tamayo, P., Mootha, V. K., Mukherjee, S., Ebert, B. L., Gillette, M. A., Paulovich, A., Pomeroy, S. L., Golub, T. R., Lander, E. S. et al. (2005). Gene set enrichment analysis: a knowledge-based approach for interpreting genome-wide expression profiles. *Proc. Natl. Acad. Sci. USA* **102**, 15545-15550. doi:10.1073/pnas.0506580102

Thiery, J. P., Acloque, H., Huang, R. Y. J. and Nieto, M. A. (2009). Epithelial-mesenchymal transitions in development and disease. *Cell* **139**, 871-890. doi:10.1016/j.cell.2009.11.007

Torborg, C. L. and Feller, M. B. (2005). Spontaneous patterned retinal activity and the refinement of retinal projections. *Prog. Neurobiol.* **76**, 213-235. doi:10.1016/j.pneurobio.2005.09.002

Torres, M., Gomez-Pardo, E. and Gruss, P. (1996). Pax2 contributes to inner ear patterning and optic nerve trajectory. *Development* **122**, 3381-3391.

Tsuji, N., Kita, K., Ozaki, K., Narama, I. and Matsuura, T. (2012). Organogenesis of mild ocular coloboma in FLS mice: failure of basement membrane disintegration at optic fissure margins. *Exp. Eye Res.* **94**, 174-178. doi:10.1016/j.exer.2011.12.004

van Nostrand, J. L., Brady, C. A., Jung, H., Fuentes, D. R., Kozak, M. M., Johnson, T. M., Lin, C.-Y., Lin, C.-J., Swiderski, D. L., Vogel, H. et al. (2014). Inappropriate p53 activation during development induces features of CHARGE syndrome. *Nature* **514**, 228-232. doi:10.1038/nature13585

Wang, Z., Divanyan, A., Jourd'heuil, F. L., Goldman, R. D., Ridge, K. M., Jourd'heuil, D. and Lopez-Soler, R. I. (2018). Vimentin expression is required for the development of EMT-related renal fibrosis following unilateral ureteral obstruction in mice. *Am. J. Physiol. Renal. Physiol.* **315**, F769-F780. doi:10.1152/ajprenal.00340.2017

Williamson, K. A. and Fitzpatrick, D. R. (2014). The genetic architecture of microphthalmia, anophthalmia and coloboma. *Eur. J. Med. Genet.* **57**, 369-380. doi:10.1016/j.ejmg.2014.05.002

Yan, W., Han, P., Zhou, Z., Tu, W., Liao, J., Li, P., Liu, M., Tian, D. and Fu, Y. (2014). Netrin-1 induces epithelial-mesenchymal transition and promotes hepatocellular carcinoma invasiveness. *Dig. Dis. Sci.* **59**, 1213-1221. doi:10.1007/s10620-013-3016-z

Zagozewski, J. L., Zhang, Q. and Eisenstat, D. D. (2014). Genetic regulation of vertebrate eye development. *Clin. Genet.* **86**, 453-460. doi:10.1111/cge.12493

Zeisberg, M. and Neilson, E. G. (2009). Biomarkers for epithelial-mesenchymal transitions. *J. Clin. Invest.* **119**, 1429-1437. doi:10.1172/JCI36183

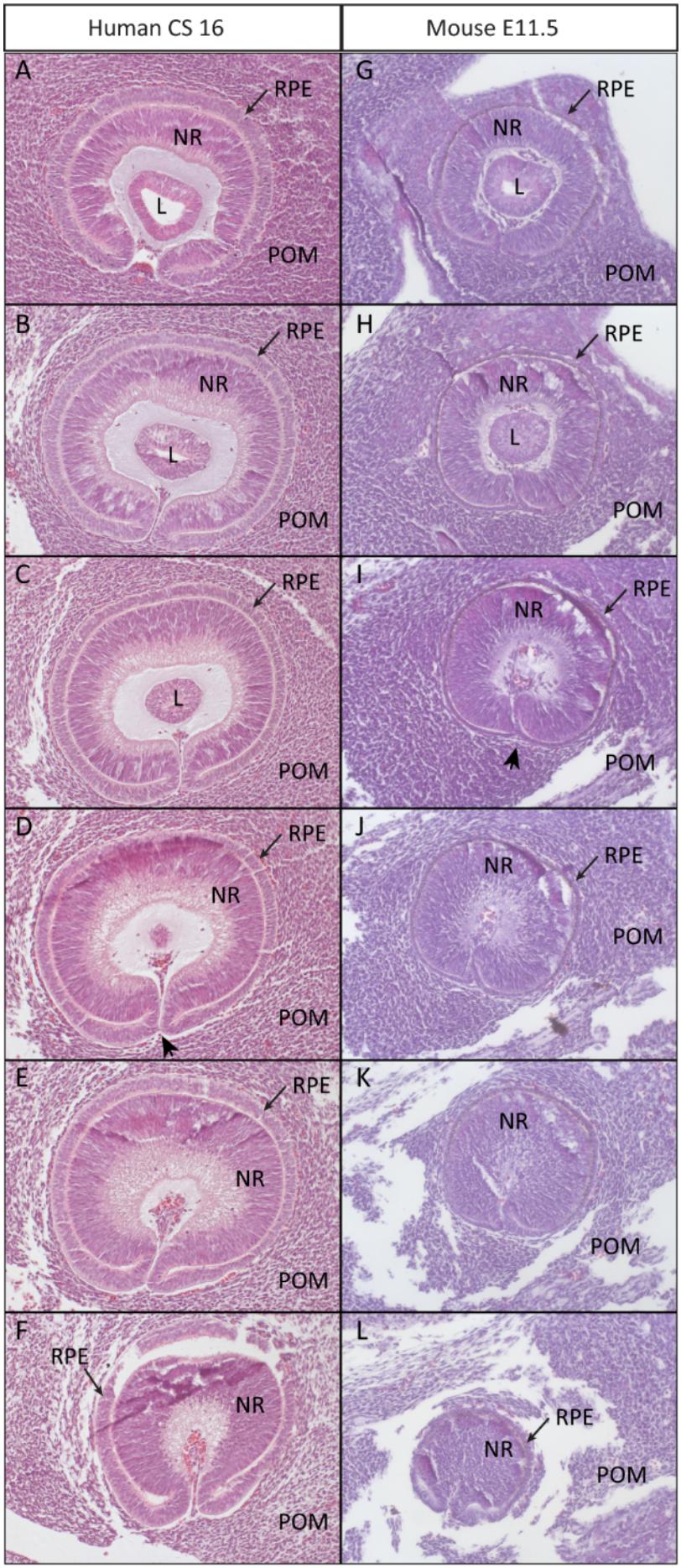

Figure S1.

A-F: Serial sections through the optic fissure of a human embryonic eye at CS16 (Day 37) from anterior to posterior. **G-L**: Serial sections through the optic fissure of a mouse embryonic eye at E11.5 from anterior to posterior. The point of initiation of fissure closure is located immediately posterior to the developing lens in both human and mouse (D & I; arrowheads). At CS16 there remained a physical gap between the fissure margins except at the initiation point. NR: Neural retina (inner layer of optic cup); RPE: Retinal pigmented epithelium (outer layer of optic cup); POM: periocular mesenchyme; L: lens.

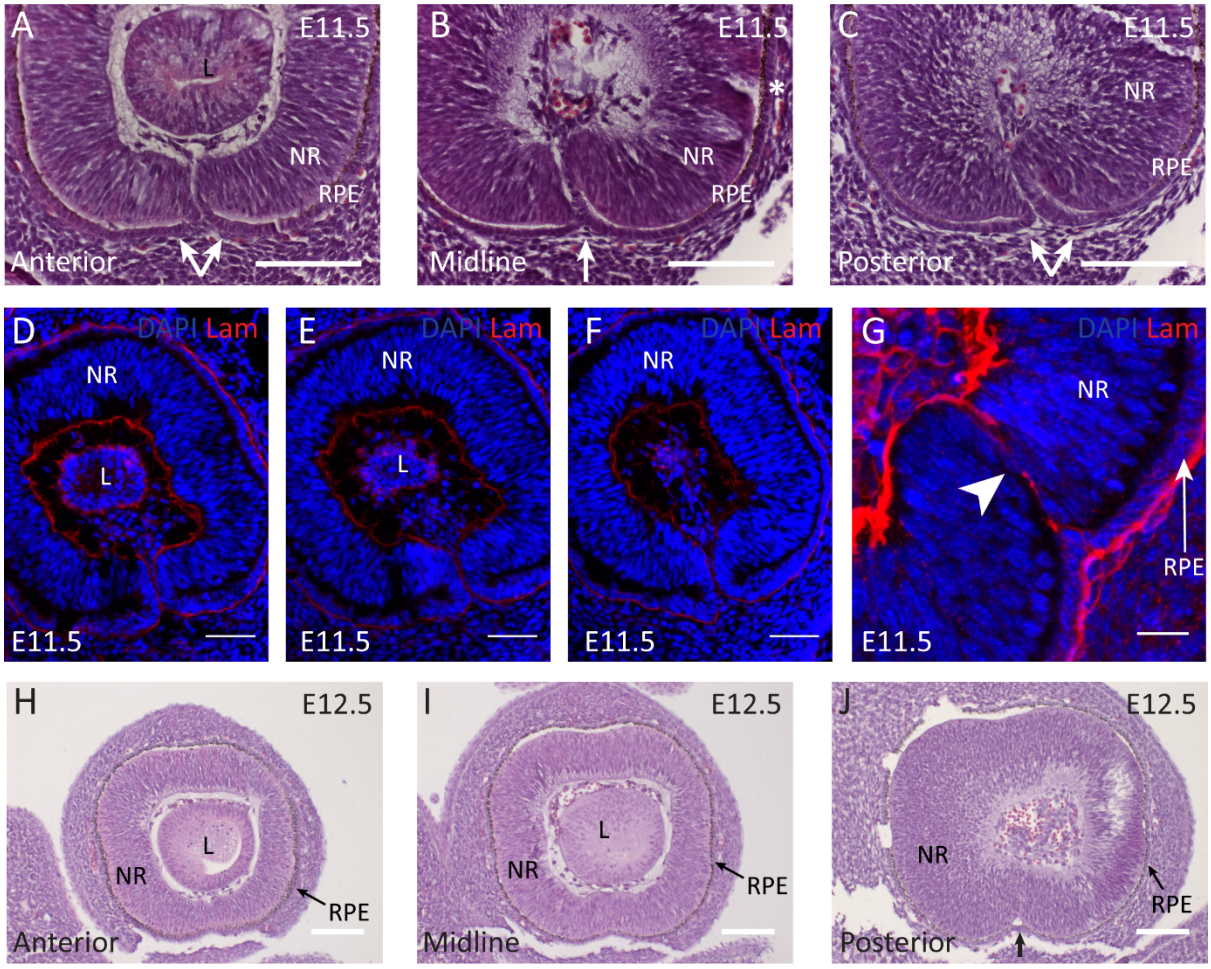

Figure S2.

A-C: Analysis of serial sections of developing mouse eyes at E11.5 (n=4) showed fissure closure had been initiated at the midpoint of the fissure at this developmental stage (B, arrow). Anterior and posterior to the point of closure, the margins were in contact but closure had not been initiated (A, C double arrows). **D-G**: Immunostaining for Laminin (red), a component of basement membrane shows the two fissure margins approach each other through their basal aspects. Discontinuous staining for laminin was observed at the point of closure (G, arrowhead) indicating a fragmentation of the basement membrane. **H-J**: Analysis of serial sections at E12.5 (n=3) showed that closure was complete along nearly the whole length of the fissure leaving a ventral indentation in the neural retina towards the posterior of the eye (G, arrow)

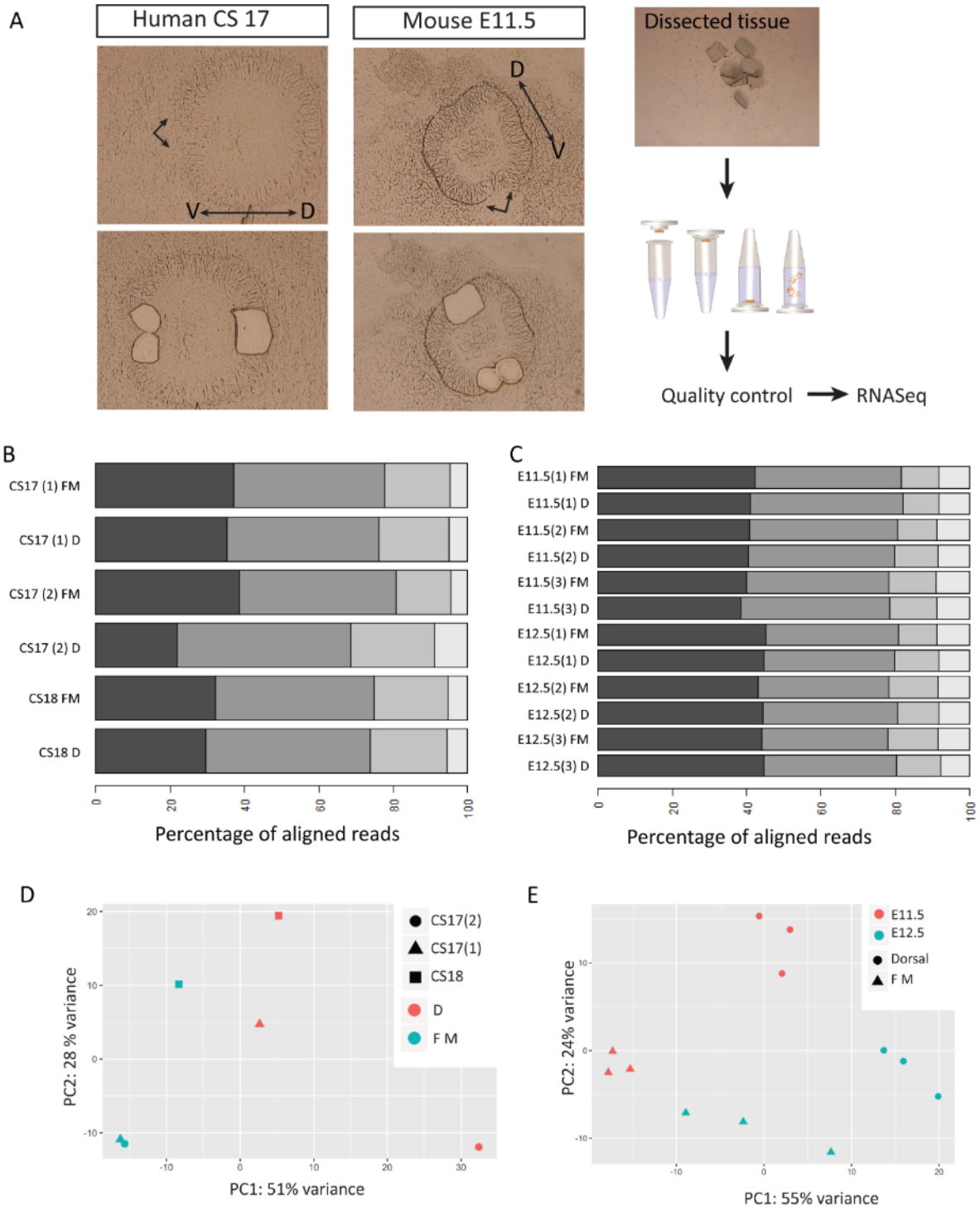

Figure S3. A: Schematic showing the process of Laser Capture Microdissection. **B:** Percentage of aligned RNA sequencing reads from human samples. **C:** Percentage of aligned RNA sequencing reads from mouse samples. The majority of reads in all samples aligned to coding and UTR regions. One sample CS17 (2) D showed some evidence of degradation. **D, E**: Principal component analysis of human and mouse RNA sequences respectively.

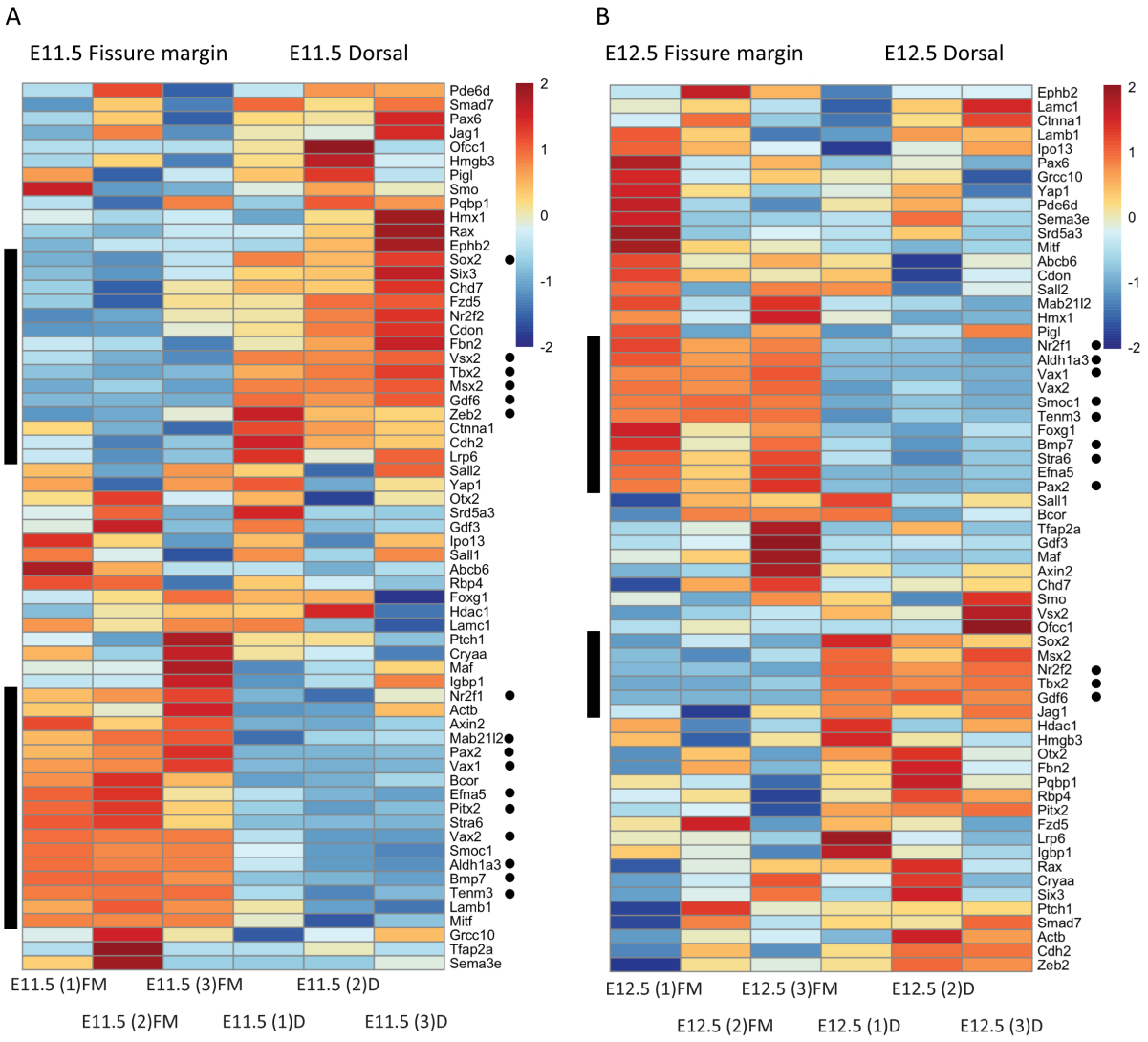

Figure S4.

A: Expression patterns of known coloboma genes (mouse orthologues of human coloboma disease genes and genes from animal models) in the E11.5 fissure margin and dorsal optic cup samples. **B**: Expression of known coloboma genes (mouse orthologues of human coloboma disease genes and genes from animal models) in the E12.5 fissure margin and dorsal optic cup samples. Black bars indicate groups of genes showing differential expression between the two regions, either enriched or suppressed in the fissure compared to the dorsal region; these groups are smaller at E12.5 than at E11.5. Black dots indicate genes that passed significance threshold in differential expression analysis.

A

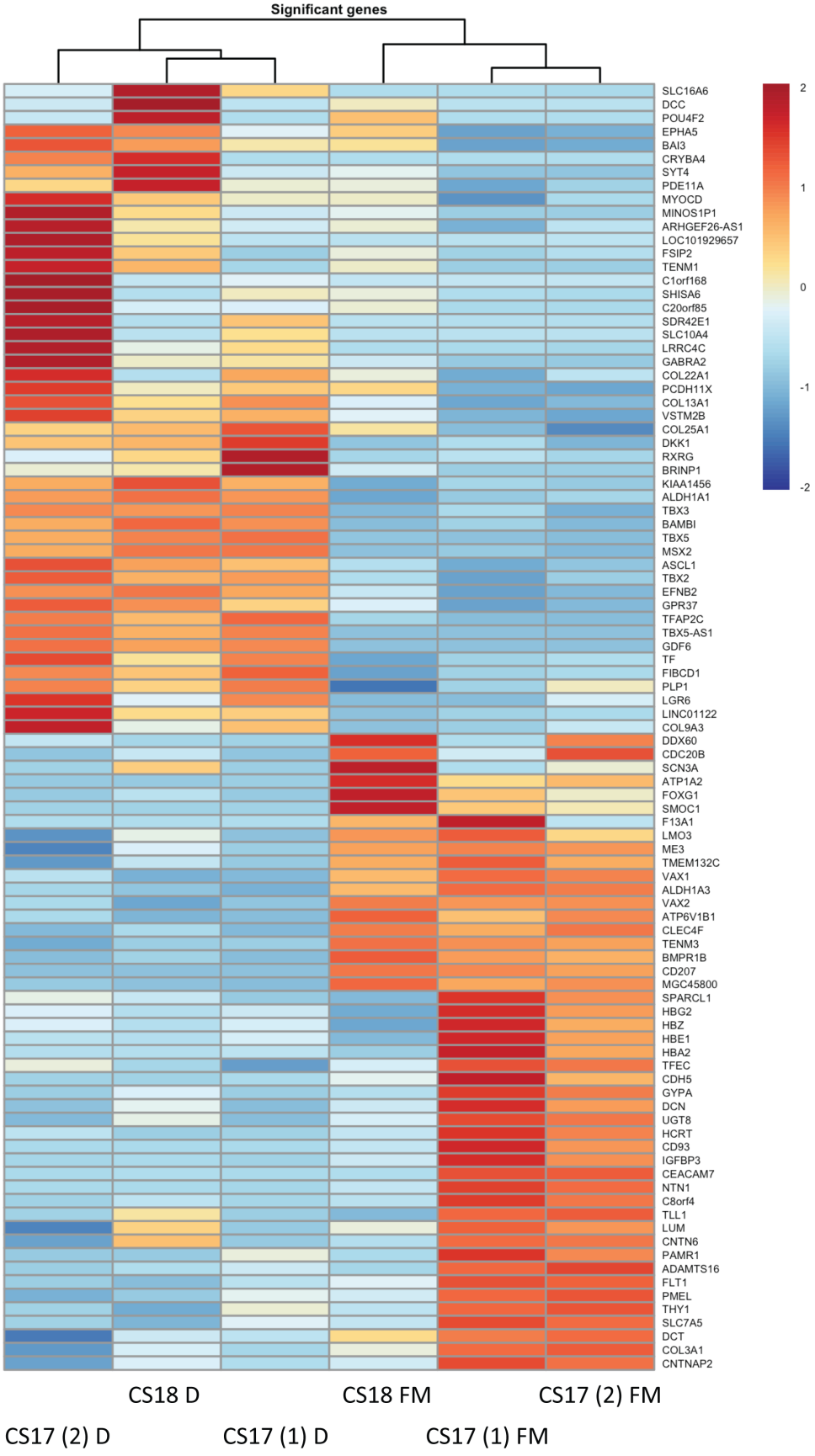

Figure S5

A: Heat map showing the top 50 significantly fissure enriched and dorsal enriched genes in the human samples.

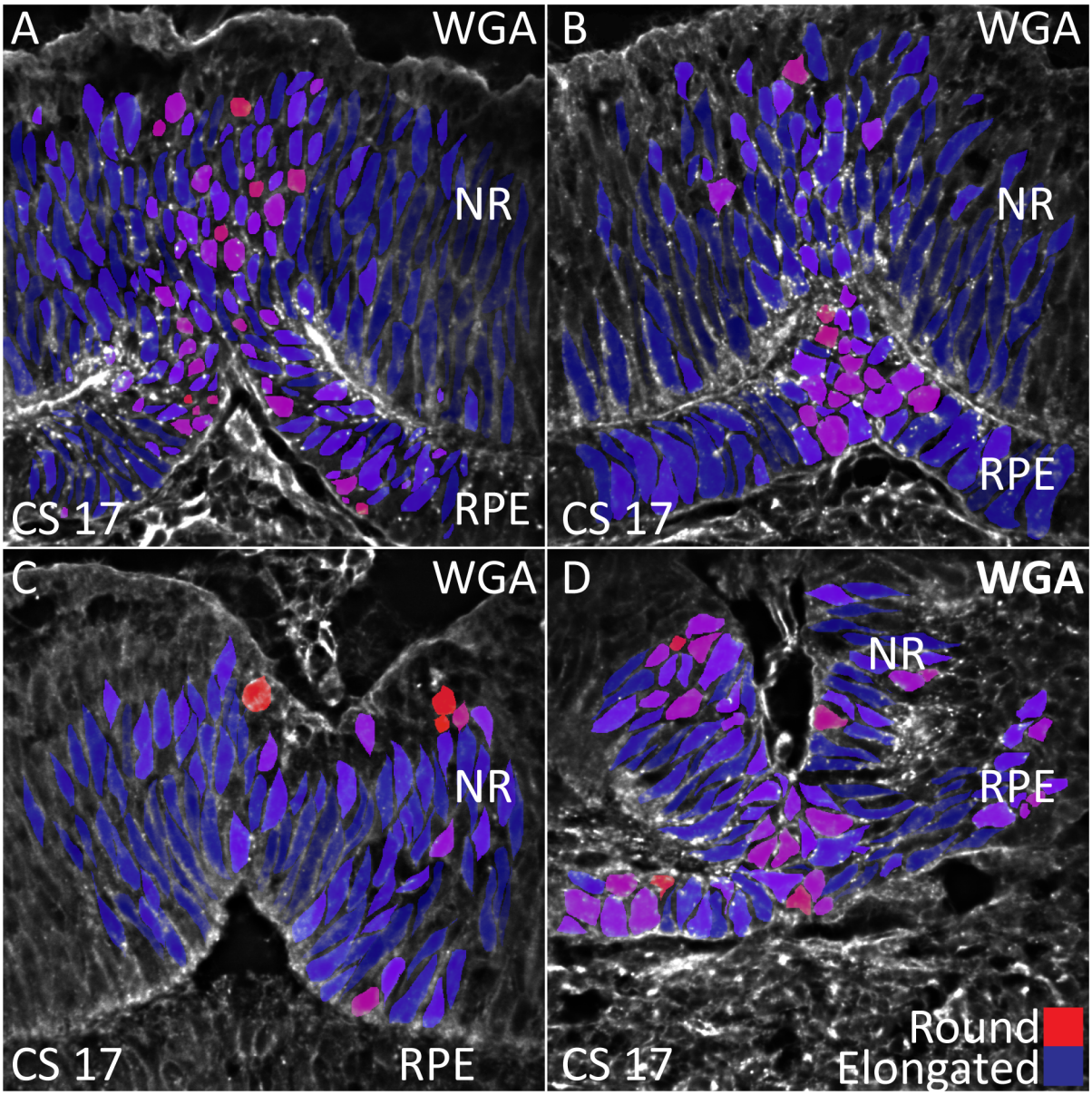

Figure S6

Cell roundness heatmaps of serial sections (anterior to posterior) of the optic fissure in a CS 17 (Day 41) human eye. Colours of the heatmap range from blue (elongated) to red (rounded). Cell membranes are labelled with WGA. **A**: Fissure margins are remodelling and cells at the margins have a rounded morphology. Cells distant from the fissure margin have elongated morphologies typical of a pseudo-stratified epithelium. **B**: At the point of closure rearranging cells have a rounded morphology. **C**: Closure is complete and cells have an elongated morphology, markedly in the presumptive NR. **D**: At the posterior closure point cells at the fissure margins show a rounded morphology. WGA: Wheat Germ Agglutinin, NR: Neural Retina, RPE: Retinal Pigmented Epithelium. Note: Sections in B and D are also shown in Figure 4F-G' and in Figure 6 E-F with Phalloidin staining.

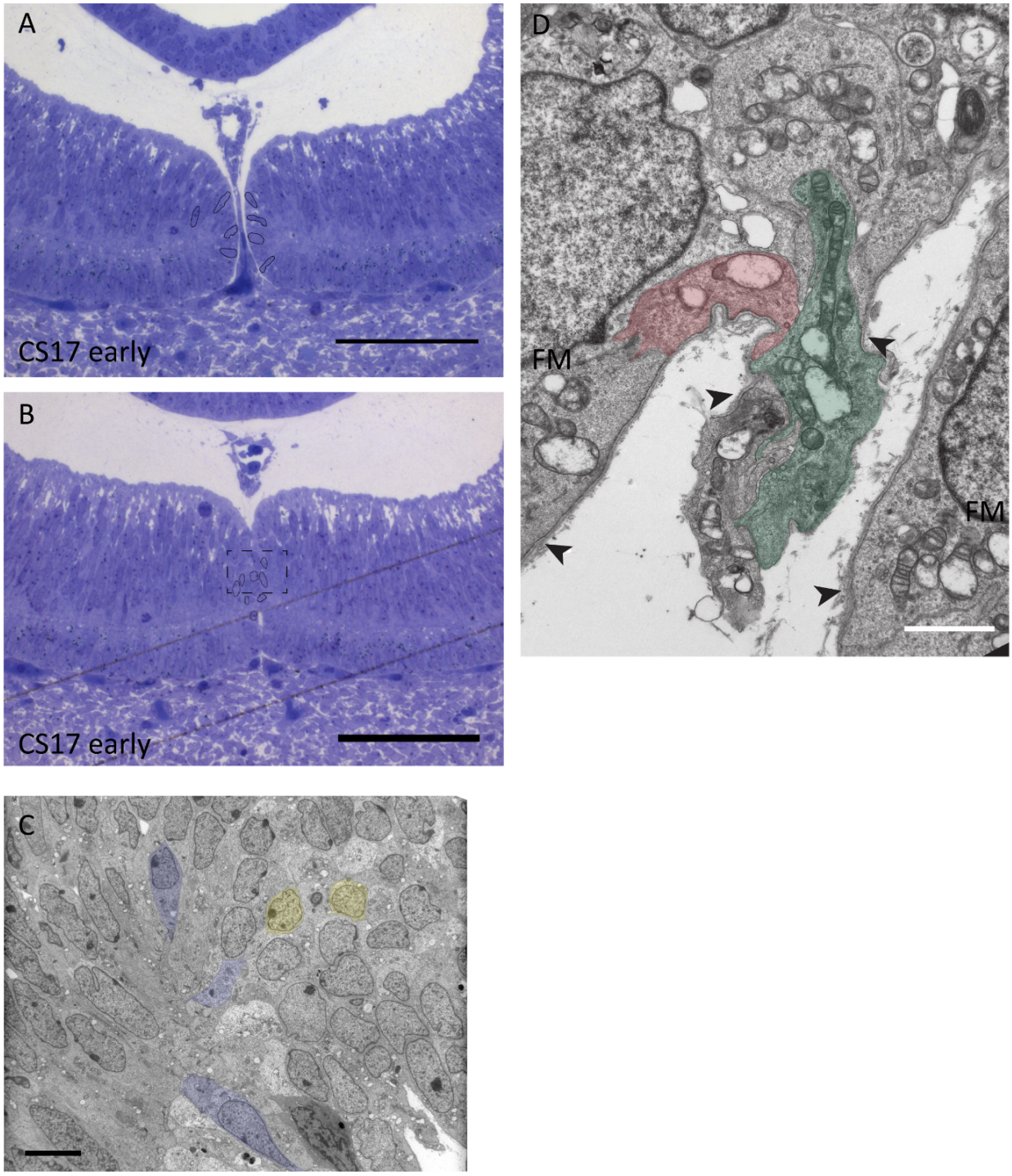

Figure S7. A, B: Histological sections showing the human optic fissure margins before and during closure at CS17. Selected nuclei are outlined to illustrate the change in morphology of the cells. **C:** Electron micrograph at the point of closure in a human eye showing both elongated (blue) and rounded (yellow) cells. **D:** High magnification electron micrograph showing cellular material being extruded at the fissure margins. Arrowheads indicate basement membrane. Red and blue indicate two selected cells.

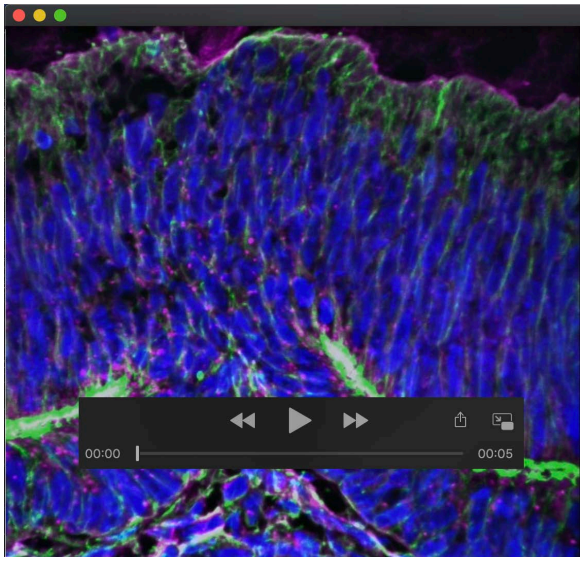

Movie 1: 3D projection of a section of the fissure margins immediately anterior to the anterior point of closure of a CS17 human eye. Blue: DAPI, Green: Phalloidin, Magenta: WGA (Wheat Germ Agglutinin, labelling cell membranes). Cells at the fissure margins have a rounded morphology.

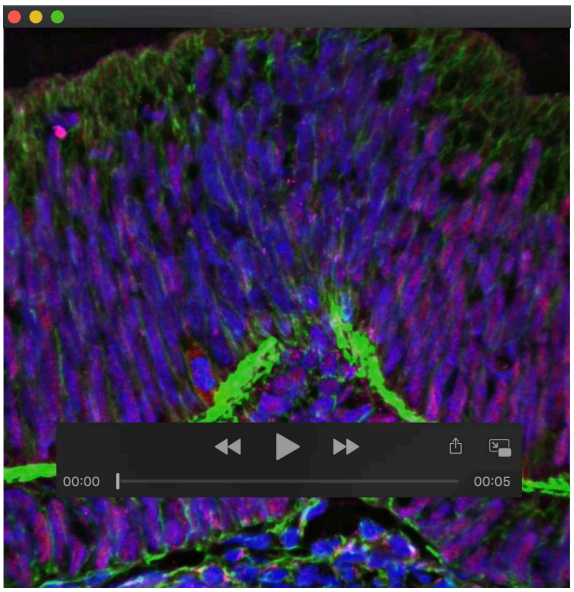

Movie 2: 3D projection of a section of the fissure margins at the anterior point of closure of a CS17 human eye. Blue: DAPI, Green: Phalloidin, Red: PAX6, Magenta: WGA (Wheat Germ Agglutinin, labelling cell membranes). Rearranging cells have a distinct rounded morphology.

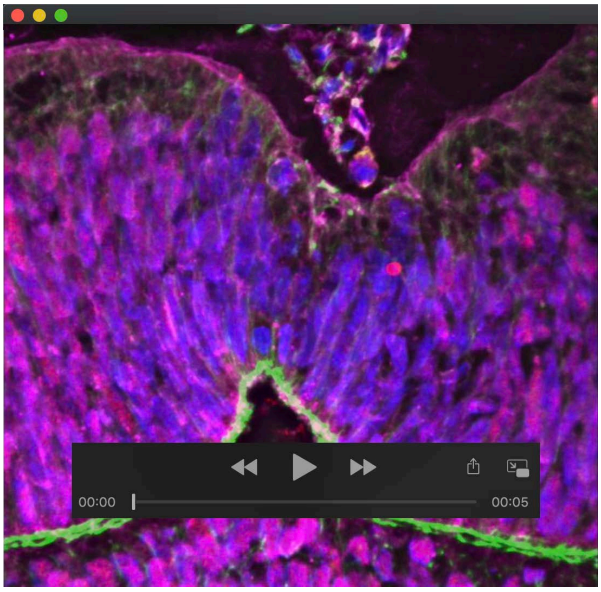

Movie 3: 3D projection of a section of the fissure margins immediately posterior to the anterior point of closure of a CS17 human eye. Blue: DAPI, Green: Phalloidin, Red: PAX6, Magenta: WGA (Wheat Germ Agglutinin, labelling cell membranes). In this region closure is complete and cells have elongated morphologies.

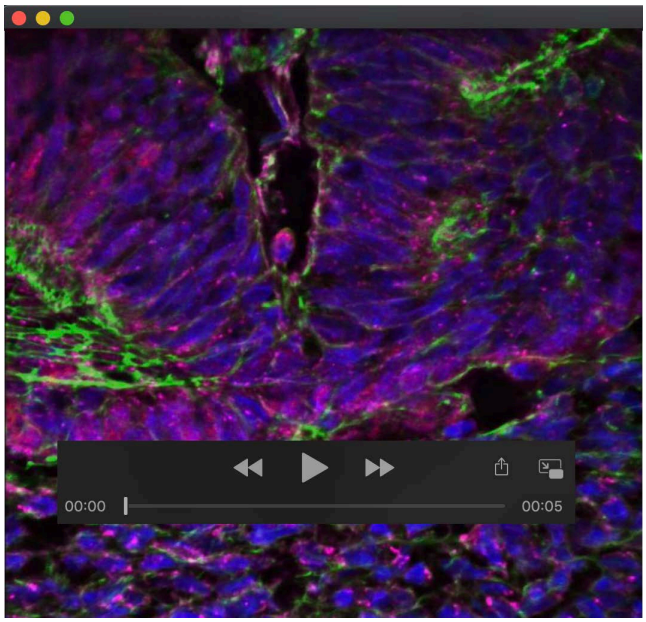

Movie 4: 3D projection of a section of the fissure margins at the posterior point of closure of a CS17 human eye. Blue: DAPI, Green: Phalloidin, Red: PAX6, Magenta: WGA (Wheat Germ Agglutinin, labelling cell membranes). Puncta of strong phalloidin staining are visible in cells at the point of closure.

Table S1. Mouse fissure and dorsal enriched genes at E11.5

Click here to Download Table S1

Table S2. Mouse fissure and dorsal enriched genes at E12.5

Click here to Download Table S2

Table S3. Gene ontology terms represented by fissure and dorsal enriched genes in E11.5 mouse eyes

Click here to Download Table S3

Table S4. Gene ontology terms represented by fissure and dorsal enriched genes in E12.5 mouse eyes

Click here to Download Table S4

Table S5. Hallmark gene sets positively and negatively correlated with the fissure margins.

Click here to Download Table S5

Table S6. All significantly differentially expressed genes

Click here to Download Table S6

LIAO, Y., SMYTH, G. K. & SHI, W. 2014. featureCounts: an efficient general purpose program for assigning sequence reads to genomic features. *Bioinformatics,* 30**,** 923-30.

LIBERZON, A., BIRGER, C., THORVALDSDOTTIR, H., GHANDI, M., MESIROV, J. P. & TAMAYO, P. 2015. The Molecular Signatures Database (MSigDB) hallmark gene set collection. *Cell Syst,* 1**,** 417-425.

LOVE, M. I., ANDERS, S., KIM, V. & HUBER, W. 2015. RNA-Seq workflow: gene-level exploratory analysis and differential expression. *F1000Res,* 4**,** 1070.

O'RAHILLY, R. & MULLER, F. 1987. *Developmental stages in human embryos : including a revision of Streeter's "Horizons" and a survey of the Carnegie Collection,* Washington, D.C., Carnegie Institution of Washington.

SAGE, D., DONATI, L., SOULEZ, F., FORTUN, D., SCHMIT, G., SEITZ, A., GUIET, R., VONESCH, C. & UNSER, M. 2017. DeconvolutionLab2: An open-source software for deconvolution microscopy. *Methods,* 115**,** 28-41.

SUBRAMANIAN, A., TAMAYO, P., MOOTHA, V. K., MUKHERJEE, S., EBERT, B. L., GILLETTE, M. A., PAULOVICH, A., POMEROY, S. L., GOLUB, T. R., LANDER, E. S. & MESIROV, J. P. 2005. Gene set enrichment analysis: a knowledge-based approach for interpreting genome-wide expression profiles. *Proc Natl Acad Sci U S A,* 102**,** 15545-50.